Non-perturbative modelling of energetic particle effects on resistive wall mode: Anisotropy and finite orbit width

Yueqiang Liu, I. T. Chapman, J. P. Graves, G. Z. Hao, Z. R. Wang, J. E. Menard, M. Okabayashi, E. J. Strait, and A. Turnbull

Citation: Physics of Plasmas **21**, 056105 (2014); doi: 10.1063/1.4872307
View online: https://doi.org/10.1063/1.4872307
View Table of Contents: http://aip.scitation.org/toc/php/21/5
Published by the American Institute of Physics

Non-perturbative modelling of energetic particle effects on resistive wall mode: Anisotropy and finite orbit width[a)]

Yueqiang Liu,[1,b),c)] I. T. Chapman,[1] J. P. Graves,[2] G. Z. Hao,[3] Z. R. Wang,[4] J. E. Menard,[4] M. Okabayashi,[4] E. J. Strait,[5] and A. Turnbull[5]
[1]*Euratom/CCFE Fusion Association, Culham Science Centre, Abingdon OX14 3DB, United Kingdom*
[2]*Ecole Polytechnique Federale de Lausanne (EPFL), Centre de Recherches en Physique des Plasmas, Association EURATOM-Confederation Suisse, 1015 Lausanne, Switzerland*
[3]*Southwestern Institute of Physics, PO Box 432, Chengdu 610041, China*
[4]*Princeton Plasma Physics Laboratory, Princeton University, PO Box 451, Princeton, New Jersey 08543-0451, USA*
[5]*General Atomics, P.O. Box 85608, San Diego, California 92186-5608, USA*

(Received 25 November 2013; accepted 11 February 2014; published online 25 April 2014)

A non-perturbative magnetohydrodynamic-kinetic hybrid formulation is developed and implemented into the MARS-K code [Liu *et al.*, Phys. Plasmas **15**, 112503 (2008)] that takes into account the anisotropy and asymmetry [Graves *et al.*, Nature Commun. **3**, 624 (2012)] of the equilibrium distribution of energetic particles (EPs) in particle pitch angle space, as well as first order finite orbit width (FOW) corrections for both passing and trapped EPs. Anisotropic models, which affect both the adiabatic and non-adiabatic drift kinetic energy contributions, are implemented for both neutral beam injection and ion cyclotron resonant heating induced EPs. The first order FOW correction does not contribute to the precessional drift resonance of trapped particles, but generally remains finite for the bounce and transit resonance contributions, as well as for the adiabatic contributions from asymmetrically distributed passing particles. Numerical results for a 9MA steady state ITER plasma suggest that (i) both the anisotropy and FOW effects can be important for the resistive wall mode stability in ITER plasmas; and (ii) the non-perturbative approach predicts less kinetic stabilization of the mode, than the perturbative approach, in the presence of anisotropy and FOW effects for the EPs. The latter may partially be related to the modification of the eigenfunction of the mode by the drift kinetic effects. [http://dx.doi.org/10.1063/1.4872307]

I. INTRODUCTION

Advanced tokamak operation, such as that foreseen for the ITER 9MA scenario,[1] aims at high beta plasma regimes beyond the no-wall Troyon limit[2] for the ideal kink instability. The high beta plasma is, on one hand, desirable for more economic fusion power production (the fusion power production is proportional to the square of beta) and steady state operation (by increasing the fraction of plasma self-sustained bootstrap current), but on the other hand, more difficult to achieve. The most prominent obstacle is probably due to the onset of the resistive wall mode (RWM).[3] This macroscopic instability, of the magnetohydrodynamic (MHD) origin, causes a global distortion of the plasma that often results in a major disruption. Understanding the damping physics of the RWM is the key for reliable prediction of the mode stability in ITER, and possibly in the future high beta DEMO designs as well.

Because the RWM originates from the ideal kink instability, it is conventionally studied within the framework of the ideal MHD theory. However, despite the fact that the mode's structure (especially the radial displacement) still resembles that of an ideal kink, the growth rate of the RWM is greatly reduced by the presence of a resistive wall located sufficiently close to the plasma surface—in fact, the mode's growth time becomes the same order as the typical wall eddy current decay time in nominal situations. The wall time is normally several milliseconds in present day tokamaks, and reaches a fraction of second in ITER. Therefore, the RWM time scale is much longer than that of the ideal kink instability, which typically grows in microsecond time scale.

This orders of magnitude slower growth time makes the RWM different from the ideal kink mode in many aspects. For instance, it is much more practical to design a feedback scheme to actively control the RWM instability, than directly control the ideal kink instability. A more profound consequence, in terms of the mode damping physics, is the accessibility of the RWM to the kinetic resonant damping regimes at various particle drift frequencies. In these regimes, the RWM can no longer be treated as a sole ideal MHD mode—a drift kinetic description of the mode is needed,[4] in addition to certain continuum resonances induced damping described by the fluid theory.[5,6]

We emphasize that, unlike other MHD modes, the RWM basically does not rotate together with the plasma—the (complex) frequency of the mode stays in the same order as the inverse wall time in the laboratory frame. As a consequence, the resonant condition holds predominantly between the plasma toroidal rotation frequency (the Doppler-shifted mode frequency) and the drift frequencies of plasma

[a)]Paper BI2 6, Bull. Am. Phys. Soc. **58**, 23 (2013).
[b)]Invited speaker.
[c)]E-mail: yueqiang.liu@ccfe.ac.uk

particles. This is true of course only when the plasma rotation frequency is larger than the mode frequency. In the opposite case, both plasma rotation frequency and the mode frequency (as measured in the laboratory frame) are important for the drift kinetic resonances.

The kinetic theory for the RWM has recently been extensively developed, including both analytic study[4,7–9] and numerical simulations in full toroidal geometry.[10–15] A MHD-kinetic hybrid formulism is normally adopted in these studies. Two approaches are envisaged within this hybrid formulation. In the so called perturbative approach, the eigenfunction of the fluid RWM (or sometimes the ideal kink mode) is loaded into a kinetic code, in order to evaluate the perturbed drift kinetic potential energy δW_k. The latter is then inserted into a RWM dispersion relation[4] based on the extended energy principle, yielding a prediction for the RWM stability in the presence of the kinetic effects. This approach has been adopted in several of the major kinetic RWM codes, such as MISK,[13,16] MISHKA + HAGIS,[11] and MARS-K.[10] In addition, MARS-K also adopts a non-perturbative approach, in which the drift kinetic equation is solved together with the MHD equations (see Sec. II), thus allowing correction to the RWM eigenfunction across the whole plasma by the kinetic effects. The AEGIS-K[17] code is a full kinetic code that has been used for studying the kinetic effects on the RWM.[18] Since this code is based on a gyrokinetic formulation[19] that correctly recovers the ideal MHD limit, AEGIS-K is hybrid in appearance but kinetic in essence. The key element in the gyrokinetic formulation[19] is to solve both the equilibrium and perturbed Vlasov equations to sufficient orders (as well as retaining certain gyrophase-dependent part of the perturbed distribution function), such that essentially both the equilibrium and the perturbed Pfirsch-Schlüter currents are correctly recovered.

Unlike many other MHD modes (e.g., the internal kink instability, or the toroidal Alfvén eigenmode) that often interact with energetic particles (EPs), the RWM can be subject to essential kinetic effects from both thermal and energetic particles, mainly due to the rather low frequency of the mode in the laboratory frame. This opens various possible resonance regimes between the mode and particles, depending on the toroidal plasma flow speed. The kinetic effects of thermal particles (both ions and electrons) are relatively easy to be studied, thanks to the fact that (i) the equilibrium distribution of thermal particles is usually well described by a Maxwellian, and hence is isotropic in the particle pitch angle space; (ii) the finite orbit effects (e.g., the finite banana width of trapped thermal ions) are normally negligible partially thanks to the global mode structure (in terms of the plasma displacement) of the RWM.[10]

The kinetic effects from EPs, on the other hand, require a deeper investigation, due to possible anisotropy and asymmetry[20] in the (equilibrium) distribution of particles, and potentially the finite orbit width (FOW) corrections due to the magnetic drift.[20] The latter issue is probably less severe for a global mode such as the RWM, compared to MHD modes whose eigenfunctions (displacement) experience more sharp radial variations (e.g., the internal kink mode[21]). Yet still, for realistic toroidal modelling, it is important to consider the FOW corrections of EPs in the RWM study. For this purpose, the MARS-K code has recently been updated to include the capability of modelling both the anisotropy and FOW effects of EPs for the RWM study. Moreover, these effects are cast in a non-perturbed hybrid formulation, as reported in this work. We mention that anisotropy of energetic particles has been previously considered in MISK code calculations for NSTX[13] and that the anisotropy and FOW effects are (naturally) incorporated into particle guiding centre following codes such as HAGIS, and perturbative toroidal simulations of the RWM stability including these effects have recently been performed using MISHKA + HAGIS, in particular, for ITER plasmas.[15] In the context of the RWM modelling, the major difference between the MISK or MISHKA + HAGIS and the MARS-K formulations is that the latter allows the non-perturbative approach.

Section II describes the non-perturbative MHD-kinetic hybrid formulation in full toroidal geometry, with both anisotropy and FOW effects of EPs included. Certain interesting physics aspects associated with this formulation are also discussed. Section III reports numerical benchmarking between MARS-K and MISHKA + HAGIS. As a numerical example, we apply the new MARS-K code to an ITER 9MA steady state plasma, with results reported in Sec. IV. Section V draws conclusion and discussion.

II. FORMULATION

A. MHD-kinetic hybrid formulation

The MARS-K formulation, introduced in Ref. 10, couples the linearised MHD equations for the plasma momentum balance and the single fluid Ohm's law to the perturbed pressure tensor, which is evaluated by solving the drift kinetic equation for the perturbed distribution functions for various particle species. A generic subsonic toroidal flow is also included into the formulation. The toroidal flow (for thermal ions in the single fluid description) includes an equilibrium $\mathbf{E}\times\mathbf{B}$ flow and the ion diamagnetic flow, where $\mathbf{E}$ and $\mathbf{B}$ are the equilibrium electrostatic and magnetic fields, respectively. The subsonic $\mathbf{E}\times\mathbf{B}$ flow also enters into the perturbed distribution functions as solutions of the drift kinetic equation. The hybrid formulation, in the full toroidal geometry, is described by the following set of equations in the Eulerian frame:

$$(\gamma + in\Omega)\boldsymbol{\xi} = \mathbf{v} + (\boldsymbol{\xi}\cdot\nabla\Omega)R^2\nabla\phi, \tag{1}$$

$$\begin{aligned}\rho(\gamma + in\Omega)\mathbf{v} = &-\nabla\cdot\mathbf{p} + \nabla\times\mathbf{Q}\times\mathbf{B} + \nabla\times\mathbf{B}\times\mathbf{Q}\\ &-\rho\left[2\Omega\nabla Z\times\mathbf{v} + (\mathbf{v}\cdot\nabla\Omega)R^2\nabla\phi\right]\\ &-\nabla\cdot(\rho\boldsymbol{\xi})R^2\Omega^2\nabla Z\times\nabla\phi,\end{aligned} \tag{2}$$

$$(\gamma + in\Omega)\mathbf{Q} = \nabla\times(\mathbf{v}\times\mathbf{B}) + (\mathbf{Q}\cdot\nabla\Omega)R^2\nabla\phi, \tag{3}$$

$$\mathbf{p} = p_{||}\hat{\mathbf{b}}\hat{\mathbf{b}} + p_{\perp}(\mathbf{I} - \hat{\mathbf{b}}\hat{\mathbf{b}}), \tag{4}$$

$$p_{||} = \sum_j \int M_j v_{||}^2 f_j^1 d\Gamma, \quad p_{\perp} = \sum_j \int \frac{1}{2} M_j v_{\perp}^2 f_j^1 d\Gamma, \tag{5}$$

where the fluid quantities $\boldsymbol{\xi}, \mathbf{v}, \mathbf{Q}$ represent the plasma displacement, perturbed velocity, and perturbed magnetic field,

respectively. ρ is the unperturbed plasma density. Ω is the angular frequency of the equilibrium flow of the plasma along the toroidal angle ϕ. The linear problem is formulated as an eigenvalue problem, with γ being the eigenvalue. n is the toroidal mode number of the perturbation with respect to an axi-symmetric toroidal equilibrium. (R, ϕ, Z) represents the cylindrical coordinate system for the torus. A conventional unit system is assumed with the vacuum permeability $\mu_0 = 1$. The Eulerian formulation is useful when the resistive plasma model is considered, which is the case in the generic MARS-K formulation. But for the RWM study, we normally neglect the plasma resistivity.

We point out that, since our hybrid formulation is partly based on the standard single fluid description of the plasma, the toroidal rotation $\mathbf{\Omega}$ represents the bulk ion rotation, which is the sum of the $\mathbf{E} \times \mathbf{B}$ flow and the bulk ion diamagnetic flow. These two flows are not separable in the single fluid description. On the other hand, in the Braginskii two-fluid formulation,[22] or in certain extended MHD formulations that keep the separation between the $\mathbf{E} \times \mathbf{B}$ flow and the diamagnetic flow, the so-called gyroviscous cancellation[23] results in a diamagnetic correction to the inertia term in the fluid equations, representing a finite Larmor radius (FLR) effect. This FLR correction to the plasma inertia is also recovered in the gyrokinetic formulation from Ref. 19, together with other FLR correction terms of the same order.

Note that even though the diamagnetic correction is neglected in the plasma inertia, the ω_* terms are fully retained in the drift kinetic resonance operators. Neglect of ω_* correction for the plasma inertia is probably reasonable for the RWM, for which the inertia plays a minor role (up to certain limits) in the mode's stability. In fact, most of the perturbative analysis (e.g., Ref. 4) drops the plasma inertia term in the RWM dispersion relation. For other MHD modes where the plasma inertia is essential (e.g., the internal kink mode[24]), it is critical to keep the diamagnetic correction mentioned above, probably together with other FLR terms as derived in Refs. 19 and 24 as well, although it has also been argued that the (stabilizing) role of the FLR correction to the plasma inertia can be defeated by the collisionless dissipation due to drift resonances of particles.[25]

One may argue that the diamagnetic correction from energetic ions may be more important than bulk ions for the plasma inertia. However, if we assume that the equilibrium pressure contributed by EPs is smaller than that by the bulk ions, we have $n_{EP}\omega_{*EP} \sim P_{EP} < n_i\omega_{*i} \sim P_i$. Therefore, we can still neglect EP's FLR correction to the plasma inertia if we make a similar approximation for bulk ions.

The perturbed kinetic pressure tensor $\mathbf{p}$ includes both parallel (to the equilibrium magnetic field), $p_{||}$, and perpendicular, $p_\perp$, components. Here, $\mathbf{I}$ is the unit tensor, and $\hat{\mathbf{b}} \equiv \mathbf{B}/B, B \equiv |\mathbf{B}|$. Γ denotes the velocity space of particles, and j denotes the particle species including thermal ions and electrons as well as energetic ions. We assume that the thermal particles are distributed in equilibrium by a Maxwellian distribution, and the energetic particles can have various equilibrium distributions to be specified in Sec. II B. The perturbed distribution function for each particle species, f_j^1, is the solution of the perturbed drift kinetic equation, which we solve together with the fluid equations. The solution procedure for the drift kinetic equation, with the inclusion of the first order FOW correction, will be described in Sec. II C. We emphasize here that the unknown eigenvalue γ of the above linear problem also enters into the drift kinetic solution f_j^1 via various types of kinetic resonances. Furthermore, the eigenfunction of the system, in terms of the perturbations $\boldsymbol{\xi}_\perp, \mathbf{Q}$, also enters into the drift kinetic equations as unknown quantities. The perturbed pressure tensor $\mathbf{p}$ couples back to the momentum equation (2). We refer to this self-consistently coupled system of equations as a non-perturbative hybrid formulation. The other way of viewing this non-perturbative approach is that it provides a drift kinetic closure to the single fluid MHD equations.

On the other hand, MARS-K can also solve the hybrid system in a perturbative way as the other kinetic RWM codes.[11,13] In the perturbative formulation, the code first solves the fluid equations as an eigenvalue problem, with the drift kinetic equation for the pressure tensor replaced by the state equation of an ideal gas, for the perturbed scalar pressure. The eigenfunction, as well as the eigenvalue, of the fluid equation is then inserted into the drift kinetic equation for f_j^1, in order to further evaluate the perturbed pressure tensor and the perturbed drift kinetic energy. The latter is eventually used to assess the kinetic effects on the RWM stability in the perturbative approach by using an analytic dispersion relation.

Before proceeding further to describe the drift kinetic solution, we make three important remarks on the validity conditions of this hybrid formulation.

First, the formulation is only valid at subsonic plasma flows due to two reasons: (i) MARS-K only couples to a static equilibrium solver even in the presence of the equilibrium flow. Usually, a subsonic flow introduces minor modifications to the corresponding static equilibrium, since the correction terms are proportional to the square of the sound Mach number; (ii) our drift kinetic formulation is valid only at subsonic flows. Note that in the complete absence of the equilibrium flow, the hybrid formulation fully decouples from the perturbed parallel velocity (and parallel displacement as well), as opposed to the standard single fluid MHD formulation, where the parallel motion always couples in via the compressibility term in the equation of state for the perturbed scalar pressure. The decoupling of the hybrid formulation from the parallel momentum equation occurs, because the parallel motion of particles is now fully described by the drift kinetic equation. However, a finite flow introduces inertial terms that again couple back to the parallel displacement in the fluid equations, despite certain partial cancellations.[26] This results in two potential problems with our hybrid formulation. One is the legality of introducing the parallel fluid velocity in a formulation where the parallel motion of the particles is now fully described by the drift kinetic equation as mentioned above. The other, more fundamental, problem is associated with the parallel sound wave resonance, which is described by the projection of Eq. (2) along the equilibrium magnetic field line. It is known that this fluid description of the sound wave resonance, in the presence of near-sonic plasma flow, is unphysical[27] and should be

replaced by the kinetic treatment such as the guiding center plasma model.[28] In the MARS-K implementation, we consider two possible ways to resolve the aforementioned inconsistency. One is to introduce a key in the code to turn off the centrifugal and coriolis terms in the momentum equation (2), thus avoiding coupling to $\mathbf{v}_{||}$ even in the presence of equilibrium flow. This is similar to the treatment adopted in Ref. 18. The other way is to add a parallel viscous term $-\rho\kappa_{||}|k_{||}v_{th,i}|[\mathbf{v}+(\boldsymbol{\xi}\cdot\nabla)\mathbf{V}_0]_{||}$ to the momentum equation (2),[29–32] where $k_{||}$ is the parallel wave number for the perturbation, $v_{th,i}$ is the thermal speed of bulk ions, $\mathbf{V}_0 = R^2\Omega\nabla\phi$. The fluid parallel sound wave resonance is effectively damped by choosing a sufficiently large numerical parameter $\kappa_{||}$. With the hybrid formulation, we also numerically tested the effect of coupling to the parallel fluid velocity by keeping the full centrifugal and coriolis terms, and neglecting the parallel viscous term. As long as the equilibrium flow is strongly subsonic, the effects due to this coupling are normally small.

Second, our formulation so far neglects the connection to electrostatic modes and, in particular, it is assumed that $\delta\mathbf{E}_{||} = 0$. To include this effect, an equation associated with the neutrality condition needs to be added to the hybrid system, if we were to include the perturbed electrostatic potential.

Third, while the anisotropy of the EP equilibrium distribution is correctly taken into account in solving the perturbed distribution function (and hence in calculating the perturbed anisotropic pressure), our equilibrium solution still assumes an isotropic equilibrium pressure. The anisotropy of equilibrium pressure may introduce new types of instabilities, which are beyond the scope of the present work. Without a rigorous consideration of the anisotropy in the equilibrium solution, the present formulation is approximately valid when the anisotropic EP's pressure fraction is relatively small, or the anisotropy is relatively weak.

B. Anisotropy of EP distribution

In the perturbative drift kinetic analysis, known equilibrium distribution functions are prescribed for particle species. In the previous version of the MARS-K implementation,[10] we assume a Maxwellian equilibrium distribution for thermal ions as well as electrons. For EPs, we assume a slowing down distribution which is isotropic in particle pitch angle. This EPs model is probably reasonable for representing the fusion born alphas, but far too crude for describing beam or rf wave induced EPs distribution.

In this work, we consider equilibrium distribution models that are anisotropic in the particle pitch angle. These models are primarily designed for EPs, but can also be used for thermal particles in the new MARS-K implementation. For reasons of numerical efficiency, these models are all based on parametrized analytic expressions, as functions of the radial equilibrium flux label ψ, the particle energy ε, and the particle pitch angle $\Lambda \equiv v_\perp^2 B_0/(v^2 B)$, where B_0 is the amplitude of the equilibrium field strength, B, evaluated at the magnetic axis, $v_\perp$ and v are the perpendicular and full velocities, respectively, of the particle.

One such model is similar to that proposed in Ref. 33, which has been used to describe EPs distribution from negative neutral beam injection (NBI) in one of the latest ITER designs. This model has an overall slowing down distribution in the particle energy space, combined with the Gaussian models for the particle pitch angle distribution

$$\hat{f}^0(\psi,\varepsilon,\zeta) = \frac{C(\psi)}{\varepsilon^{3/2}+\varepsilon_c^{3/2}}\frac{1}{2\sqrt{\pi}\delta\zeta}\sum_i C_i \exp\left[-\frac{(\zeta-\zeta_i)^2}{\delta\zeta^2}\right], \quad (6)$$

where $\zeta = v_{||}/v$, and ε_c corresponds to the crossover velocity of the EP. The Gaussian width weakly depends on the particle energy

$$\delta\zeta^2(\psi,\varepsilon) = \delta\zeta_0^2 - \frac{1}{3}\ln\left[\frac{\varepsilon^{3/2}(1+\varepsilon_c^{3/2}/\varepsilon_a^{3/2})}{\varepsilon^{3/2}+\varepsilon_c^{3/2}}\right], \quad (7)$$

where $\varepsilon_a(\psi)$ is the EP's birth energy, which we assume to be finite. The constant $\delta\zeta_0$ is a tunable parameter of the model. With $\delta\zeta_0 \to \infty$, we recover the isotropic distribution model as that used in Ref. 49.

The other sets of parameters (C_i, ζ_i) can be used to specify various types of distribution functions. For instance, a co-tangential injection model[33] for ITER is obtained by setting $\{C_i\} = \{2, 2, -1, -1\}$, and the corresponding $\{\zeta_i\} = \{\zeta_0,\ 2-\zeta_0, 2\zeta_+ - \zeta_0, 2\zeta_+ - 2 + \zeta_0\}$, for co-passing particles; $\{C_i\} = \{1, 1\}$ and $\{\zeta_i\} = \{2\zeta_- + \zeta_0, 2\zeta_- + 2 - \zeta_0\}$ for counter-passing particles; $\{C_i\} = \{1, 1, 1, 1\}$ and $\{\zeta_i\} = \{\zeta_0,\ 2-\zeta_0, -\zeta_0, -2+\zeta_0\}$ for trapped particles. Here, ζ_+ (ζ_-) denotes the boundary between trapped and co-(counter-)passing particles in the pitch angle space, and ζ_0 is yet another tunable parameter of the model. For the ITER NNBI induced EPs, it was found that a choice of $\zeta_0 = 0.8$, $\delta\zeta_0^2 = 0.015$ reasonably well reproduces the TRANSP simulated particle distribution[33] in ITER. These are also the values that we use for the co-tangential NBI model for our ITER simulations, to be reported in Sec. IV. Other combinations of (C_i, ζ_i) are also envisaged in MARS-K, in order to describe normal NBI or even counter-NBI induced EPs.

Figure 1 shows the particle distribution along the pitch angle ζ, for an ITER 9MA steady state plasma to be studied in this paper, with the same choice of parameters $\zeta_0 = 0.8$, $\delta\zeta_0^2 = 0.015$, for particles located at the minor radius of $s \equiv \psi_p = 0.8$ (ψ_p is the normalized equilibrium poloidal flux), with the particle energy level of $\varepsilon/\varepsilon_a = 0.5$. Note that the co-passing particles (with positive ζ) dominate in this distribution. There is an asymmetry in the distribution between co- and counter-passing particles. The trapped particles always have a symmetric distribution with respect to $\zeta = 0$ according to this model.

In MARS-K, we generally assume that the flux surface averaged radial density and pressure profiles for each species of EPs are known and enter into the code as the input. We then solve an inverse problem to find the two free functions $\{(C(\psi), \varepsilon_a(\psi)\}$ in the above model, giving the analytic expressions (6) and (7) of the distribution function.

We shall further refer to the above EPs equilibrium distribution model simply as the (anisotropic) NBI model, to

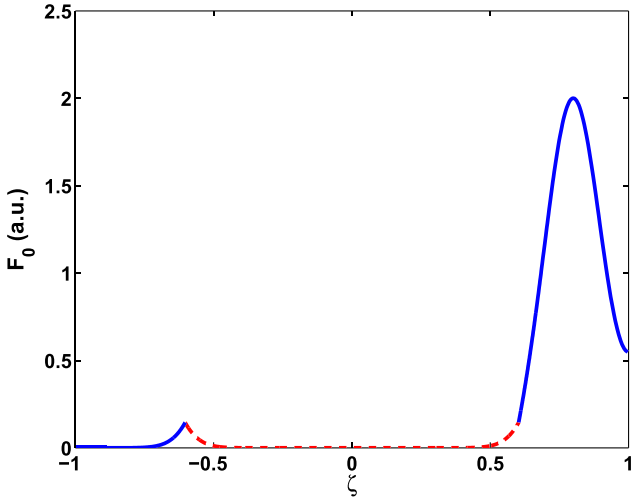

FIG. 1. Example of an anisotropic, asymmetric equilibrium distribution of the co-NBI induced EPs, based on an ITER equilibrium. The solid (dashed) line indicates the passing (trapped) particles.

distinguish it from the next, what we call the ICRH (ion cyclotron resonant heating) model that has also been implemented into the MARS-K code. This ICRH model, proposed in Ref. 34, is based on a Bi-Maxwellian distribution, and is reasonably well suited for describing the ICRH driven EPs

$$\hat{f}^0(\psi,\varepsilon,\Lambda) = C(\psi)[1+\sigma S(\psi,\Lambda)]\frac{\nu_T^{1/2}(\psi)}{T_\perp^{3/2}(\psi)} \times \exp\left[-\frac{\varepsilon}{T_\perp}\left(\frac{\Lambda}{h_c}+\nu_T(\psi)\left|1-\frac{\Lambda}{h_c}\right|\right)\right], \quad (8)$$

where $\nu_T(\psi) = T_\perp(\psi)/T_{||}(\psi)$ is the ratio of the perpendicular, $T_\perp$, to the parallel (with respect to equilibrium magnetic field lines), $T_{||}$, equilibrium temperatures for the EP, and $\sigma = \text{sign}(v_{||})$. The asymmetry factor S generally depends on both particle pitch angle and the minor radius. One example is $S(\psi,\Lambda) = S_0(\psi)(1-\Lambda^2/h_{\min}^2)^2$, where $S_0(\psi)$, as well as the temperature anisotropy factor $\nu_T(\psi)$, is numerically specified as the input of the model. The S-factor is valid only for $0 \le \Lambda \le h_{\min}$, i.e., for passing particles. Here, $h_{\min}(\psi)$ is the minimal value of $h \equiv B_0/B$ along the poloidal angle at a given flux surface. We assume that $S=0$ for trapped particles. This specification of S ensures a smooth transition from an asymmetric pitch angle distribution for passing particles, to a symmetric distribution for trapped particles.

The exponential factor in expression (8) defines the anisotropy of the particle distribution along the pitch angle Λ. The parameter h_c (a constant) specifies the radial location of the ICRH wave resonance inside the plasma. In the limit of $\nu_T(\psi) = 1, S_0(\psi) = 0$, and a sufficiently large value of h_c (so that the ICRH wave resonance moves outside the plasma), this model recovers the standard isotropic Maxwellian distribution.

Similar to the NBI model, we generally compute the two unknown coefficients $\{C(\psi), T_\perp(\psi)\}$ by solving an inverse problem, with the surface averaged particle density and pressure profiles specified as the input. Of course for cases where these two coefficients can be directly specified, this inverse solution procedure is not necessary.

The above anisotropic (and asymmetric) distribution models allow more realistic modelling of the kinetic effects of EPs on the RWM in present day and future fusion devices. Given these equilibrium distributions, the next step is to compute the perturbed distribution function by solving the perturbed drift kinetic equation (in full toroidal geometry). The solution of the perturbed distribution function is conventionally represented as sum of an adiabatic part and a non-adiabatic part. It is important to note that for a generic anisotropic equilibrium distribution, the adiabatic part of the perturbed pressure should also be "kinetically" evaluated, and be used to replace the fluid convection term.

In the following, we derive both adiabatic and non-adiabatic kinetic solutions that are convenient, more importantly efficient, for being included into a non-perturbative MHD-kinetic hybrid formulation with FOW corrections. We assume a generic anisotropic, asymmetric equilibrium distribution, and start with the non-adiabatic part.

C. FOW correction to non-adiabatic kinetic solution

The derivation of the drift kinetic formulation for MARS-K, with the inclusion of the FOW effects, closely follows that by Graves.[35] We have carried out the derivations separately for passing and trapped particles. But shall only show the derivations for passing particles below, followed by comments highlighting certain subtle elements when applying the similar approach for trapped particles.

Similar to Ref. 10, we start with the perturbed drift kinetic equation for the non-adiabatic solution $f_L^{1\sigma}$, as derived by Porcelli[36]

$$\frac{df_L^{1\sigma}}{dt} = \left.\frac{\partial f^{0\sigma}(P_\phi,\varepsilon,\Lambda)}{\partial\varepsilon}\right|_{P_\phi,\Lambda}\frac{\partial H^{1\sigma}}{\partial t} - \left.\frac{\partial f^{0\sigma}(P_\phi,\varepsilon,\Lambda)}{\partial P_\phi}\right|_{\varepsilon,\Lambda}\frac{\partial H^{1\sigma}}{\partial\phi}, \quad (9)$$

where we have explicitly assigned $\sigma \equiv \text{sign}(v_{||})$ to both to the equilibrium distribution f^0 and the perturbed function f_L^1, as well as the perturbed particle Lagrangian $H^1 \equiv -[Mv_{||}^2\xi_\perp\cdot(\hat{\mathbf{b}}\cdot\nabla)\hat{\mathbf{b}} + \mu(|Q| + \xi_\perp\cdot\nabla B)]$, emphasizing the asymmetry of distributions for passing particles. Here, $\mu = Mv_\perp^2/(2B)$ is the magnetic moment of the particle, and the first order approximation of the perturbed field amplitude is $|Q| \simeq Q_{||} \equiv \mathbf{Q}\cdot\hat{\mathbf{b}}$. The above equation needs to be solved for each particle species separately. But we suppress the additional subscript "j" denoting the particle species, wherever no confusion is caused.

Equation (9) was derived from the Vlasov equation utilizing Littlejohn's Lagrangian.[37] It is reasonable to treat energetic ions as collisionless species. The equilibrium distribution function $f^{0\sigma}$ is defined as a function of constants of the particle motion: the toroidal canonical angular momentum $P_\phi = -Ze\psi + MR^2\dot{\phi}$, the particle energy ε, and the particle pitch angle Λ. In Ref. 36, a solution of Eq. (9) was derived retaining full FOW effects. But unfortunately that solution requires full drift orbit tracing for each particle, and

hence would result in prohibitively demanding computations when inserted into the MHD-kinetic hybrid formulation.

In this work, we seek a solution that takes into account the lowest order FOW correction. By doing so, we arrive at an equation for the perturbed drift kinetic pressure, that has the same order of complexity in terms of numerical implementations, as well as require the same order of computational efforts, compared to our previous formulation without the FOW effect.[10] In order to further simplify the derivations, without losing significant physics effects, we only keep the orbit width corrections in quantities with strong radial variations, i.e., the perturbed fluid quantities $\xi_\perp, Q_{||}$, etc., and the equilibrium distribution function f^0 itself. The FOW corrections due to radial variation of other equilibrium quantities (e.g., the field strength B and the equilibrium metrics tensors associated with the flux based curvilinear coordinate system) are neglected. We mention that a perturbative formulation, with the first order FOW correction, has been implemented in the NOVA-K code.[39]

Before proceeding to the solution of Eq. (9), we note a subtle issue in prescribing the particle equilibrium distribution function $f^{0\sigma}$ as the constant of motion P_ϕ, or equivalently, the quantity $\tilde{\psi} \equiv -P_\phi/Ze$. It is clear that one can add a constant $\psi_0(\psi, \varepsilon, \Lambda)$ to $\tilde{\psi}$, resulting in another constant of motion $\hat{\psi} = \tilde{\psi} + \psi_0$. Whilst in the Littlejohn-Porcelli theory, the equilibrium distribution function f^0 is specified using the constant of motion $\tilde{\psi}$, it is known that the quantity $\hat{\psi}$, with a proper choice of ψ_0, is used in order to correctly recover the neoclassical theory,[38] in particular, the bootstrap currents due to passing particles.[35] The necessity of including neoclassical modifications for MHD mode studies has been clearly demonstrated in Ref. 19. In this work, we shall follow both definitions of the constant of motion, $\tilde{\psi}$ and $\hat{\psi}$, and the resulting approach will be simply called the $\tilde{\psi}$-approach and the $\hat{\psi}$-approach, respectively. As will be shown later, these two approaches result in almost exactly the same final expressions for the perturbed kinetic pressure tensor, except one term.

Neglecting the drift correction in particle toroidal velocity $\dot{\phi}$, and defining $\Delta\psi \equiv \psi - \hat{\psi} = \psi - \psi_0 - \tilde{\psi}$, we have

$$\tilde{\psi} = \psi - \frac{FB_0}{\Omega_c^0}\frac{v_{||}}{B}, \quad \Delta\psi = \frac{FB_0}{\Omega_c^0}\frac{v_{||}}{B} - \psi_0, \tag{10}$$

where $F(\psi)$ is the equilibrium poloidal current flux function ($\mathbf{B} = F\nabla\phi + \psi \times \nabla\phi$), and $\Omega_c^0 = ZeB_0/M$. For cases where energetic ions predominantly experience drag on background electrons and ions, the solution of the Fokker-Planck equation for the equilibrium distribution function yields[35]

$$\psi_0 = \frac{FB_0}{\Omega_c^0}\left\langle\frac{v_{||}}{B}\right\rangle, \tag{11}$$

where $\langle\cdot\rangle$ denotes the surface average. In the opposite limit, where the pitch scattering dominates (often the case for thermal ions in the banana regime), we have

$$\psi_0 = \frac{FB_0}{\Omega_c^0}\varepsilon\int_\Lambda^{h_{\min}} \frac{\langle v_{||}/B\rangle}{\langle v_{||}^2/B\rangle} d\Lambda', \tag{12}$$

which leads to an exact recovery of the bootstrap current from the neoclassical theory.[35]

Further on, we shall search for the solution of Eq. (9), with the lowest order FOW correction, by expanding both the perturbed particle Lagrangian $H^{1\sigma}$ and the equilibrium distribution function $f^{0\sigma}$ in terms of the small parameter $\Delta\psi$, which we also assume is the same order as ψ_0.

The first key step, as far as the FOW correction is concerned, is to expand $H^{1\sigma}$ in terms of $\Delta\psi$. The perturbed particle Lagrangian $H^{1\sigma} = H^{1\sigma}(\psi, \chi, \varepsilon, \Lambda)$ can be symbolically written as $H^{1\sigma} = -C(\psi, \chi, \varepsilon, \Lambda)\sum_m X_m(\psi)\exp(-i\omega t + im\chi + in\phi)$, where C denotes the equilibrium quantities (mixed with particle constants of motion ε and Λ), and $X \equiv \{\xi_\perp, Q_{||}\}$ denotes the perturbed fluid quantities, decomposed into the Fourier harmonics along the poloidal angle χ and the toroidal angle ϕ of the torus. Note that for the linear perturbation with respect to an axisymmetric toroidal equilibrium, we only consider a single toroidal harmonic $n \neq 0$. The eigenfrequency of the linear perturbation is ω. Also note that all the fluid quantities, both the equilibrium coefficients C and the linear perturbations X_m are functions of the flux coordinate ψ. We take the first order Taylor expansion of X_m around the constant of motion $\hat{\psi}$

$$X_m(\psi) = X_m(\hat{\psi}) + \Delta\psi X'_m(\hat{\psi}). \tag{13}$$

The above expression yields a Taylor expansion for the particle Lagrangian $H^{1\sigma}$, which now explicitly depends on σ (via the $\Delta\psi$ factor), as a function of $\hat{\psi}$. [Note that the unexpanded $H^{1\sigma}$, as a function of ψ, formally does not depend on σ.] In terms of the particle motion, both $\psi(t)$, on which the equilibrium factor C still depends, and the poloidal angle $\chi(t)$ are functions of time t, so is the Taylor expanded perturbed particle Lagrangian $H^{1\sigma}(t)$. Now we follow a standard procedure[10] of decomposing $H^{1\sigma}(t)$, as a function of particle motion, into a secular part (bounce averaged) and a bounce-periodic part (for passing particles, the bounce period becomes the transit period). We then decompose the bounce-periodic part into bounce harmonics. These procedures transfer Eq. (9) into

$$\frac{df_L^{1\sigma}(t)}{dt} = i\varepsilon\left(\omega\frac{\partial f^{0\sigma}}{\partial\varepsilon}\bigg|_{\tilde{\psi},\Lambda} - \frac{n}{Ze}\frac{\partial f^{0\sigma}}{\partial\tilde{\psi}}\bigg|_{\varepsilon,\Lambda}\right) \times \sum_{ml}\left[H_{ml}^{(0)}X_m(\hat{\psi}) + \bar{H}_{ml}^{(1)}X'_m(\hat{\psi})\right] \times \exp\left[iD_0^\sigma(\hat{\psi})t\right], \tag{14}$$

where $D_0^\sigma(\hat{\psi}) = m\langle\dot{\chi}\rangle + n\langle\dot{\phi}\rangle + l\omega_b - \omega = n\omega_d(\hat{\psi}) + \sigma[m + nq(\hat{\psi}) + l]|\omega_b| - \omega$ is the particle phase factor which does not depend on t. ω_d is the toroidal precession frequency of particles. l is the bounce harmonic number. The bounce harmonics $H_{ml}^{(0)}$ are the basic terms associated with the zero orbit width (ZOW) approximation. The bounce harmonics $H_{ml}^{(1)}$ are associated with the FOW correction. They are defined as

$$H_{ml}^{(0)} = \frac{1}{\tau_b}\int_0^{2\pi} C(\tau)\exp[im(\chi(\tau) - \langle\dot{\chi}\rangle\tau) + in(\phi(\tau) - \langle\dot{\phi}\rangle\tau) - il\omega_b\tau]d\tau,$$
$$\bar{H}_{ml}^{(1)} = \frac{1}{\tau_b}\int_0^{2\pi} \Delta\psi(\tau)C(\tau)\exp[im(\chi(\tau) - \langle\dot{\chi}\rangle\tau) + in(\phi(\tau) - \langle\dot{\phi}\rangle\tau) - il\omega_b\tau]d\tau, \quad (15)$$

where τ_b is the bounce period (i.e., transit period for passing particles).

It is important to note that so far we have not made the Taylor expansion of the equilibrium distribution function $f^{0\sigma}$ with respect to $\Delta\psi$. This means that all the terms from the right hand side of Eq. (14), except the last exponential phase factor, are functions of constants of particle motion, and therefore are independent of time t. This allows a straightforward analytic time integration of Eq. (14), yielding the solution for the perturbed distribution function $f_L^{1\sigma}$, which can then be inserted into Eq. (5) to obtain the non-adiabatic contribution for the perturbed drift kinetic pressures.

However, since all the perturbed quantities from Eqs. (1)–(5) are specified in the flux variable ψ, not in the particle constant of motion such as $\hat{\psi}$, we need to perform Taylor expansion of all quantities, including $f^{0\sigma}, X_m(\hat{\psi}), X'_m(\hat{\psi}), D_0^\sigma(\hat{\psi})$, around ψ. This consists of the second key step derivation in this FOW correction formulation.

The expansion for $X_m(\hat{\psi})$ and $X'_m(\hat{\psi})$ is straightforward

$$X_m(\hat{\psi}) = X_m(\psi) - \Delta\psi X'_m(\psi),$$
$$X'_m(\hat{\psi}) = X'_m(\psi) - \Delta\psi X''_m(\psi), \quad (16)$$

where the second order derivatives, X''_m, eventually only give the second order FOW correction, and hence drop out of the final result. The first order derivative, X'_m, however remains. A RWM in a tokamak plasma is normally associated with multiple rational surfaces. Each of these rational surfaces is associated with an inertial layer, which can be very narrow for the RWM, due to the fact that the mode's growth rate is small. [This is different from an ideal kink mode, whose growth rate is large, and hence has much wider inertial layers.] Consequently, the *poloidal* component of the plasma displacement, which is roughly proportional to the first radial derivative of the radial displacement, experiences sharp variations inside the inertial layers. The FOW correction introduces the next order radial derivative, which can result in a very singular eigenfunctions near rational surfaces. To avoid numerical difficulties, we introduce a numerical parameter (effectively the width of inertial layers) controlling how much of the kinetic contribution near rational surfaces need to be included into the MARS-K computations, when the FOW effect is considered.

The first order expansion of D_0^σ gives

$$D_0^\sigma(\hat{\psi}) = n\hat{\omega}_d + \sigma[m + nq(\psi) + l]|\omega_b| - \omega, \quad (17)$$

where $\hat{\omega}_d \equiv \omega_d(\hat{\psi}) + \sigma\Delta\psi(\psi,\chi,\varepsilon,\Lambda)q'(\psi)|\omega_b|$ represents the first order FOW corrected toroidal precession frequency of passing ions. Usually, the toroidal precession resonance is neglected for passing particles, since the dominant frequency in Eq. (17) is the transit frequency ω_b. However, this may not be true near mode rational surfaces, where the factor $(m + l) + nq(\psi)$ becomes small.[35] In the present MARS-K implementation, the precession drift resonance is neglected, together with the first order FOW correction term associated with the magnetic shear. This treatment is consistent with the truncation of the kinetic contribution near rational surfaces described above.

The first order FOW expansion of the equilibrium distribution function $f^{0\sigma}$ depends on the choice of the constant of motion for the first variable. In the $\tilde{\psi}$-approach (following the Littlejohn-Porcelli theory), where $f^{0\sigma} = f^{0\sigma}(\tilde{\psi},\varepsilon,\Lambda)$, we have

$$\left.\frac{\partial f^{0\sigma}(\tilde{\psi},\varepsilon,\Lambda)}{\partial\varepsilon}\right|_{\tilde{\psi},\Lambda} = \left.\frac{\partial\hat{f}^{0\sigma}}{\partial\varepsilon}\right|_{\psi,\Lambda} - (\Delta\psi + \psi_0)\left.\frac{\partial^2\hat{f}^{0\sigma}}{\partial\varepsilon\partial\psi}\right|_{\psi,\Lambda}, \quad (18)$$

$$\left.\frac{\partial f^{0\sigma}(\tilde{\psi},\varepsilon,\Lambda)}{\partial\tilde{\psi}}\right|_{\varepsilon,\Lambda} = \left.\frac{\partial\hat{f}^{0\sigma}}{\partial\psi}\right|_{\varepsilon,\Lambda} - (\Delta\psi + \psi_0)\left.\frac{\partial^2\hat{f}^{0\sigma}}{\partial\psi^2}\right|_{\varepsilon,\Lambda}. \quad (19)$$

In the $\hat{\psi}$-approach (following the neoclassical theory), where $f^{0\sigma} = f^{0\sigma}(\hat{\psi},\varepsilon,\Lambda)$, we have[35]

$$\left.\frac{\partial f^{0\sigma}(\hat{\psi},\varepsilon,\Lambda)}{\partial\varepsilon}\right|_{\tilde{\psi},\Lambda} = \left.\frac{\partial\hat{f}^{0\sigma}}{\partial\varepsilon}\right|_{\psi,\Lambda} - \Delta\psi\left.\frac{\partial^2\hat{f}^{0\sigma}}{\partial\varepsilon\partial\psi}\right|_{\psi,\Lambda} + \frac{\partial\psi_0}{\partial\varepsilon}\left.\frac{\partial\hat{f}^{0\sigma}}{\partial\psi}\right|_{\psi,\Lambda}, \quad (20)$$

$$\left.\frac{\partial f^{0\sigma}(\tilde{\psi},\varepsilon,\Lambda)}{\partial\tilde{\psi}}\right|_{\varepsilon,\Lambda} = \left.\frac{\partial\hat{f}^{0\sigma}}{\partial\psi}\right|_{\varepsilon,\Lambda} - \Delta\psi\left.\frac{\partial^2\hat{f}^{0\sigma}}{\partial\psi^2}\right|_{\varepsilon,\Lambda} + \frac{\partial\psi_0}{\partial\psi}\left.\frac{\partial\hat{f}^{0\sigma}}{\partial\psi}\right|_{\psi,\Lambda}. \quad (21)$$

Note that the equilibrium distribution function $\hat{f}^{0\sigma}$, in all the above expressions, is a function of $(\psi,\varepsilon,\Lambda)$, a notation consistent with that in Sec. II B. Also note that the first order FOW correction involves the second order derivatives of the equilibrium distribution function.

Since MARS-K solves the MHD equations in the poloidal Fourier space, we also expand the perturbed drift kinetic pressures $p_{||}(\psi,\chi)\exp(in\phi)$ and $p_\perp(\psi,\chi)\exp(in\phi)$ in Fourier harmonics along χ. More precisely, we shall compute the kth poloidal Fourier harmonic of $Jp_{||}$ and $Jp_\perp$, where J is the Jacobian of the flux coordinate system that we choose. Utilizing all the above Taylor expansions for $f^{0\sigma}, X_m(\hat{\psi}), X'_m(\hat{\psi}), D_0^\sigma(\hat{\psi})$, keeping only the lowest order FOW correction terms, a lengthy but straightforward derivation finally yields

$$(Jp_g)_k = \sum_{kml}\int d\Lambda\Big[\big(I^{(0)} + I^{(1)}\big)H_{ml}^{(0)}G_{kml}^{(0)g} + I^{(2)}H_{ml}^{(0)}G_{kml}^{(1)g} + I^{(3)}\big(H_{ml}^{(1)}G_{kml}^{(0)g} - H_{ml}^{(0)}G_{kml}^{(1)g}\big)\frac{X'_m}{X_m}\Big]X_m, \quad (22)$$

where "g" denotes either $||$ or $\perp$, $I^{(1)} = \hat{I}^{(1)} - \tilde{I}^{(1)}$ (see below for definitions) for the $\hat{\psi}$-approach, and $I^{(1)} = 0$ for the $\tilde{\psi}$ approach. The terms with superscript "(0)" denote the ZOW terms which recover those from Ref. 10. The terms with

superscript "(1,2,3)" are the first order FOW corrections. For completeness, we list all the factors below

$$H_{ml}^{(0)} = \frac{1}{\tau_b}\int_0^{2\pi} C(\tau)\exp[im(\chi(\tau) - \langle\dot{\chi}\rangle\tau) + in(\phi(\tau) - \langle\dot{\phi}\rangle\tau) - il\omega_b\tau]d\tau, \quad (23)$$

$$H_{ml}^{(1)} = \frac{1}{\tau_b}\int_0^{2\pi} \bar{\psi}C(\tau)\exp[im(\chi(\tau) - \langle\dot{\chi}\rangle\tau) + in(\phi(\tau) - \langle\dot{\phi}\rangle\tau) - il\omega_b\tau]d\tau, \quad (24)$$

$$G_{ml}^{(0)g} = \frac{1}{2\pi}\int_0^{2\pi} JBY_g\exp[i(m+nq+l)\omega_b t(\chi) - in\phi(\chi) - ik\chi]d\chi, \quad (25)$$

$$G_{ml}^{(1)g} = \frac{1}{2\pi}\int_0^{2\pi} \bar{\psi}JBY_g\exp[i(m+nq+l)\omega_b t(\chi) - in\phi(\chi) - ik\chi]d\chi, \quad (26)$$

$$I^{(0)} = \sum_j\sum_\sigma\int \hat{I}d\varepsilon, \quad (27)$$

$$\hat{I}^{(1)} = \sum_j\sum_\sigma\int \hat{I}\frac{Ze}{n}\frac{\partial\psi_0}{\partial\varepsilon}\frac{N_0^\sigma+\omega}{N_0^\sigma}N_1 d\varepsilon, \quad (28)$$

$$\tilde{I}^{(1)} = \sum_j\sum_\sigma\int \hat{I}\frac{(N_0^\sigma\hat{f}_\varepsilon^{0\sigma})_\psi}{N_0^\sigma\hat{f}_\varepsilon^{0\sigma}}(-\psi_0)d\varepsilon, \quad (29)$$

$$I^{(2)} = \sum_j\sum_\sigma\int \hat{I}\frac{(N_0^\sigma\hat{f}_\varepsilon^{0\sigma})_\psi}{N_0^\sigma\hat{f}_\varepsilon^{0\sigma}}(-\psi_1)d\varepsilon, \quad (30)$$

$$I^{(3)} = \sum_j\sum_\sigma\int \hat{I}\psi_1 d\varepsilon, \quad (31)$$

$$\hat{I} \equiv \frac{1}{B_0\sqrt{\pi}}\left(\frac{2\pi}{M}\right)^{3/2}\varepsilon_k^{5/2}(-\hat{f}_\varepsilon^{0\sigma})\frac{N_0^\sigma}{D_0^\sigma},\ \psi_1 \equiv \sigma\frac{F}{\Omega_c^0}\left(\frac{2\varepsilon}{M}\right)^{1/2}, \quad (32)$$

where $\bar{\psi} \equiv h\sqrt{1-\Lambda/h}$, $Y_{||} \equiv \sqrt{1-\Lambda/h}$, $Y_\perp \equiv \Lambda/(2h\sqrt{1-\Lambda/h})$, $N_0^\sigma \equiv n\omega_*^\sigma + n\omega_E - \omega$, $N_1 \equiv n\omega_{*\psi_0} + n\omega_E - \omega$, and the diamagnetic frequencies are defined as $\omega_*^\sigma \equiv \hat{f}_\psi^{0\sigma}/(Ze\hat{f}_\varepsilon^{0\sigma}), \omega_{*\psi_0} \equiv (\partial\psi_0/\partial\psi)/(Ze\partial\psi_0/\partial\varepsilon)$.

Note that all the above H- and G-factors are defined in such a way that they are independent of the particle species—the contribution from all particle species is summed together into the various I-factors that treat all the kinetic integrations in the particle energy space, together with all the kinetic resonances. This factorization of the kinetic integrals into the H, G, and I factors allows a deliberate separation of the particle phase integrations (between the particle energy and phase angle), which hugely increases the computational efficiency for this non-perturbative MHD-kinetic hybrid approach.

The term associated with the radial derivatives X_m'/X_m in Eq. (22) is due to the FOW correction to the linear perturbation (i.e., the RWM eigenfunction); the remaining first order terms are due to the FOW correction to the equilibrium distribution functions. Remarkably, the $\tilde{\psi}$-approach eventually leads to results that do not depend on ψ_0. This should actually be expected if we recall that the Littlejohn-Porcelli formulation does not specify ψ_0 at all. For the $\hat{\psi}$-approach, it can be shown that there is an important cancellation between the terms associated with $\tilde{I}^{(1)}$ and $I^{(2)}$. In fact, these two terms can be combined yielding

$$-\tilde{I}^{(1)}H_{ml}^{(0)}G_{kml}^{(0)g} + I^{(2)}H_{ml}^{(0)}G_{kml}^{(1)g} = I^{(2)}H_{ml}^{(0)}\frac{1}{2\pi}\int_0^{2\pi}\frac{\Delta\psi}{\psi_1}JBY_g\exp[i(m+nq+l)\omega_b t(\chi) - in\phi(\chi) - ik\chi]d\chi. \quad (33)$$

This cancellation also seems to play an important role in the neoclassical bootstrap current calculations due to passing particles.[35] We shall return to this point when reporting numerical results.

The derivation of the FOW correction terms for trapped particles follows the same procedure as shown above for passing particles, but differs by several subtle aspects. Below we only list important differences without repeating the actual derivation.

First, we always assume that the trapped particles have a symmetric distribution in the pitch angle space, i.e., the equilibrium distribution function f^0 does not depend on σ. Consequently, the perturbed distribution function due to trapped particles, f_L^1, does not depend on σ either.

Second, $\psi_0 = 0$ for trapped particles. Therefore, there is no need to distinguish between the $\tilde{\psi}$- and $\hat{\psi}$-approaches.

Third, the expression describing the particle-mode resonance is simplified to

$$D_0^\sigma(\hat{\psi}) = n\omega_d(\hat{\psi}) + l\omega_b - \omega, \quad (34)$$

where the precession frequency $\omega_d(\hat{\psi})$ can be evaluated using the Rosenbluth-Sloan formula,[40] which includes full drift FOW effects.

Fourth, the H-and G-factors need to be evaluated for a particle travelling in both directions along the field line (consequently, σ should not appear in the I-factors). This results in certain phase cancellations in these factors

$$H_{ml}^{(0)} = \frac{2}{\tau_b}\int_0^{\tau_b/2} C(\tau)\exp[im\chi(\tau) + in\phi(\tau)]\cos(l\omega_b\tau)d\tau, \quad (35)$$

$$H_{ml}^{(1)} = \frac{-2i}{\tau_b}\int_0^{\tau_b/2} \bar{\psi}C(\tau)\exp[im\chi(\tau) + in\phi(\tau)]\sin(l\omega_b\tau)d\tau, \quad (36)$$

$$G_{ml}^{(0)g} = \frac{1}{\pi}\int_{\chi_L}^{\chi_U} JBY_g\exp[-in\phi(\chi) - ik\chi]\cos(l\omega_b t(\chi))d\chi, \quad (37)$$

$$G_{ml}^{(1)g} = \frac{i}{\pi}\int_{\chi_L}^{\chi_U} \bar{\psi}JBY_g\exp[-in\phi(\chi) - ik\chi]\sin(l\omega_b t(\chi))d\chi, \quad (38)$$

where χ_L and χ_U correspond to the two turning points of the trapped particle along the poloidal angle. For the special case of $l = 0$, where only the precessional drift resonance

remains (see Eq. (34)), the first order FOW correction terms for H- and G-factors, Eqs. (36) and (38), respectively, vanish. This means that the first order FOW correction to the precessional drift resonance induced kinetic contributions due to trapped particles vanishes. In other words, the ZOW approximation of the precessional drift resonances is accurate up to the second order in the FOW expansion. Physically, this appears to be related to the fact that the toroidal precession of trapped particles keeps drifting into the same direction (i.e., independent of σ), and the kinetic contributions from particles travelling in opposite directions along the field line exactly cancel in the first order correction. In Subsection II D, we shall see similar cancellations for the adiabatic contributions due to the FOW effects, for trapped particles.

D. FOW correction to adiabatic kinetic solution

The adiabatic contribution from passing particles to the perturbed distribution function can be written as[36]

$$f_a^{1\sigma} = -\xi_\perp \cdot \nabla f^{0\sigma} - \frac{Q_{||}}{B}\mu\frac{\partial f^{0\sigma}}{\partial \mu}. \tag{39}$$

Keeping the lowest order FOW correction for the adiabatic part, we obtain

$$\begin{aligned} f_a^{1\sigma} = &-\left[(\xi\cdot\nabla\psi)\hat{f}_\psi^{0\sigma} + \frac{Q_{||}}{B}\Lambda\hat{f}_\Lambda^{0\sigma}\right] \\ &-\left\{\begin{array}{c}(\xi\cdot\nabla\psi)\dfrac{\partial\psi_0}{\partial\psi} + \dfrac{Q_{||}}{B}\Lambda\dfrac{\partial\psi_0}{\partial\Lambda} \\ 0\end{array}\right\}\hat{f}_\psi^{0\sigma} \\ &+\left\{\begin{array}{c}\Delta\psi \\ \Delta\psi+\psi_0\end{array}\right\}\left[(\xi\cdot\nabla\psi)\hat{f}_{\psi\psi}^{0\sigma} + \frac{Q_{||}}{B}\Lambda\hat{f}_{\psi\Lambda}^{0\sigma}\right], \end{aligned} \tag{40}$$

where the upper (lower) row corresponds to the results following the $\hat{\psi}$- ($\tilde{\psi}$-) approach. Again as expected, the results from the $\tilde{\psi}$-approach do not depend on ψ_0.

The above expression for the perturbed distribution function can then be inserted into Eq. (5) to compute the perturbed pressure tensor due to the adiabatic contributions.

Similar derivations can be made also for trapped particles. It can be shown, however, that if we assume a symmetric equilibrium distribution of trapped particles along the pitch angle, the first order FOW terms vanish due to exact cancellations (between particles travelling in opposite directions along the field line). Similar cancellations also occur for symmetrically distributed passing particles. However, for generically anisotropic, asymmetric equilibrium distributions of passing particles, such as the NBI model and the ICRH model described in Sec. II B, the first order FOW correction to the adiabatic contributions remains finite.

E. Analytic subtraction of singularities in particle phase space integrations

Various types of singularities can occur in the particle phase space integrations for the non-adiabatic kinetic contributions. Some of the integrals in the particle energy space can be analytically manipulated into the plasma dispersion function, which can be evaluated using standard libraries. However, there are other integrals that involve singularity and that cannot be converted into a standard function. In these cases, we use analytic subtraction of singularities to ensure numerical accuracy. Details of three types of such integrals are given below, as examples, for the integrals in the particle energy space, in the particle pitch angle space, and along the particle trajectory in computing the geometrical factors, respectively.

First consider an example of the bounce resonance for particle distributions with infinite birth energy (e.g., the Maxwellian distribution). This integral, in the absence of the energy dependent collisionality coefficient, can be written in a general form

$$I = \int_0^\infty \frac{F\tilde{\varepsilon}_k d\tilde{\varepsilon}_k}{\sqrt{\tilde{\varepsilon}_k}+b}, \tag{41}$$

where $b = a - i\hat{\nu}/c$, $\hat{\nu} = \nu + \mathrm{Im}(\omega)$, $a = [n\omega_E - \mathrm{Re}(\omega)]/c$, $c = l\sqrt{2T/M}\omega_b$, and ω is the (complex) mode frequency, ν the energy independent effective collisionality coefficient. The singularity in the integrand occurs when $a < 0, \hat{\nu} \to +0$ at $\tilde{\varepsilon}_k^0 = a^2$. Introducing $\tilde{\varepsilon}_k(u) = \tan(\pi u/2)$, $\hat{F}(\tilde{\varepsilon}_k) = F(\tilde{\varepsilon}_k)(\sqrt{\tilde{\varepsilon}_k} - b)(\tilde{\varepsilon}_k + a^2)$, the singular part of the integrand in Eq. (41) can be extracted and analytically performed, resulting in

$$I = \int_0^1 \frac{\hat{F}(\varepsilon_k) - \hat{F}(u_0)}{(\tilde{\varepsilon}_k - b^2)(\tilde{\varepsilon}_k + a^2)}\frac{d\tilde{\varepsilon}_k}{du}du + \frac{\ln(-a^2/b^2)}{a^2+b^2}\hat{F}(u_0), \tag{42}$$

where $u_0 = (2/\pi)\mathrm{atan}(a^2)$. The integrand of the first term from the RHS of the above Eq. (42) is now regular, and the integration is numerically performed using Gaussian quadrature rules. Note that the integral I still depends on the particle pitch angle Λ (as well as on the configuration space variables): $I = I(\Lambda)$.

A similar technique is applied to particles with finite birth energy, for which the analytic integration of the singular part contributes a term $\{2 - 2a\ln[(1+a)/(-a)] - i2a\pi\mathrm{sign}(c)\}F(\tilde{\varepsilon}_k^0)$ as $\hat{\nu} \to +0$. This term itself has a weak (logarithmic) singularity in the particle pitch angle space when $a(\Lambda_0) = -1$. This singularity is again analytically extracted in the MARS-K implementation by performing the following operations:

$$\begin{aligned} &\int G(\Lambda)H(\Lambda)\sum_j I_j(\Lambda)d\Lambda \\ &= \int G(\Lambda)H(\Lambda)\sum_j [I_j(\Lambda) - I_0^j(\Lambda)F_j(\Lambda_0^j)]d\Lambda \\ &\quad + \int \sum_j I_0^j(\Lambda)F_j(\Lambda_0^j)[G(\Lambda)H(\Lambda) - G_j(\Lambda_0^j)H_j(\Lambda_0^j)] \\ &\quad + \sum_j G_j(\Lambda_0^k)H_j(\Lambda_0^k)F_j(\Lambda_0^j)\int I_0^j(\Lambda)d\Lambda, \end{aligned} \tag{43}$$

where j denotes the particle species, $F_j(\Lambda_0^j) = 2F(\tilde{\varepsilon}_k = 1, \Lambda = \Lambda_0^j)$, and $I_0^j(\Lambda) = \ln|\Lambda - \Lambda_0^j|$. The last integral in the

above expression involves singular integrand, and is analytically evaluated as $\int_{\Lambda_1}^{\Lambda_2} I_0^j(\Lambda)d\Lambda = (\Lambda_0^j - \Lambda_1)[\ln(\Lambda_0^j - \Lambda_1) - 1] + (\Lambda_2 - \Lambda_0^j)[\ln(\Lambda_2 - \Lambda_0^j) - 1]$. The remaining integrals from the RHS of Eq. (43) only involve regular integrands in the particle pitch angle space, and are again numerically evaluated using the Gaussian quadrature rules.

Finally, for trapped particles, evaluation of the geometrical factors G and H along the particle trajectory involves integral of the type $\int C(\chi)/\sqrt{h(\chi) - \Lambda}d\chi$ along the poloidal angle χ. The technique of analytic subtraction is again applied.

Besides the aforementioned singularities, a finite plasma flow also introduces continuum resonances in the fluid part of the hybrid formulation. These continuum resonances are numerically resolved by strong packing of the radial grid near resonant surfaces in MARS-K. Without any other damping terms such as the plasma viscosity, this is possible to achieve only in the presence of a finite mode growth rate (i.e., a finite inertia). In the direct MARS-K implementation (e.g., following the non-perturbative approach), we always perform computations of the mode's eigenvalue in the unstable half-plane.

III. BENCHMARKING THE CODE

The MARS-K code, with zero orbit with approximation, has been well benchmarked against the HAGIS code for thermal particles,[10] for which the FOW effect is small as far as the RWM is concerned. For the new implementation of the FOW corrections for EPs, we again benchmark with the HAGIS computations. Note HAGIS simulates guiding centre orbits for assemble of particles with full FOW effects. Therefore, we do not expect a perfect agreement between the two codes. However, as we gradually increase the particle energy, we should see how the results of the two codes depart from each other. In the benchmark example reported below, we fix the kinetic pressure while varying the density of EPs. This allows us to vary the particle energy and thus to identify the FOW correction effect.

We choose the same Solov'ev equilibrium as we previously used,[10] with aspect ratio of 5, and with a circular cross section. No rational surfaces are associated with the $n = 1$ RWM inside the plasma for this equilibrium. The EPs are assumed to have a slowing down distribution in the particle energy space, and an isotropic distribution along the particle pitch angle (thus symmetric in $v_{||}$). The equilibrium pressure of the EPs is fixed at 50% of the thermal pressure. Figure 2 compares the computed drift kinetic energy perturbations, both the real and the imaginary parts for the adiabatic and non-adiabatic contributions, by MARS-K and HAGIS, while varying the density fraction $N_{\rm EP}/N_{\rm TH}$ of EPs with respect to the thermal electron density. Note that at $N_{\rm EP}/N_{\rm TH} = 0.5$, the particles have the same level of energy as the thermal particles, and become more energetic with decreasing of the density fraction. In both codes, the perturbed drift kinetic energy δW_k is normalized by the plasma inertia associated with the radial displacement.

For comparison, the MARS-K results without the FOW correction, and with the first order FOW correction, are both

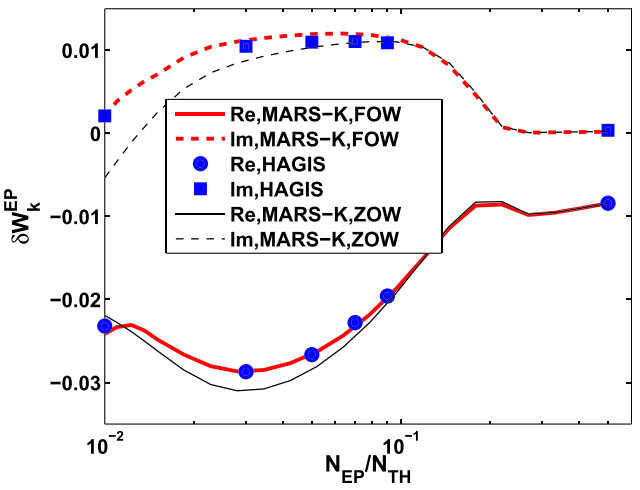

FIG. 2. Comparison of the drift kinetic energies associated with EPs, computed by MARS-K with the first order FOW correction (thick lines), with zero orbit width approximation (thin lines), and by HAGIS with full FOW drift kinetic effects (dots).

plotted. Compared are only the energy contributions from the EP species, but including all possible resonances (adiabatic, non-adiabatic precession, bounce and transit) in both codes. The no-wall ideal external kink eigenfunction is used as the linear perturbation (both codes follow the perturbative approach in this comparison). A rather fast $\mathbf{E} \times \mathbf{B}$ flow of the plasma is assumed, with $\omega_E = 0.1\omega_A$ (ω_A is the Alfvén frequency), in order to better capture the resonance effects between the mode and the particle bounce/transit motions, for which the FOW correction becomes important (we recall that the FOW correction for particle precession resonances vanishes at the first order).

Figure 2 shows a good agreement between MARS-K and HAGIS, when the first order FOW correction is taken into account in the former. In fact for this specific example, it appears that the first order correction captures most of the FOW effect for EPs, whose energy is as high as 50 times the thermal particle energy. Without the FOW correction, MARS-K results differ from that of the HAGIS prediction, and the difference generally becomes larger with increasing the particle energy, as should be expected. We notice that the drift kinetic energy δW_k also varies with the EPs density fraction at the ZOW limit. This is mainly because all the drift frequencies scale with the particle energy, which changes while varying the particle density at the fixed pressure. Consequently, the drift kinetic resonances also change. In particular, at a fixed $\mathbf{E} \times \mathbf{B}$ flow velocity, the resonances mostly occur at certain level of the particle energy. This explains the non-monotonic behaviour of δW_k on $N_{\rm EP}$. We point out that the local diamagnetic frequencies also depend on the particle energy.

Besides comparison of the results between two different codes, systematic internal benchmarking has also been carried out within MARS-K, at various limits. In particular, we report below two examples, where we recover the isotropic limits by using the anisotropic EPs models.

In obtaining the results reported in Figure 3(a), we vary the parameter $\delta\zeta_0$ specifying the width of the Gaussian functions for the anisotropic NBI model (6) and (7). In the limit

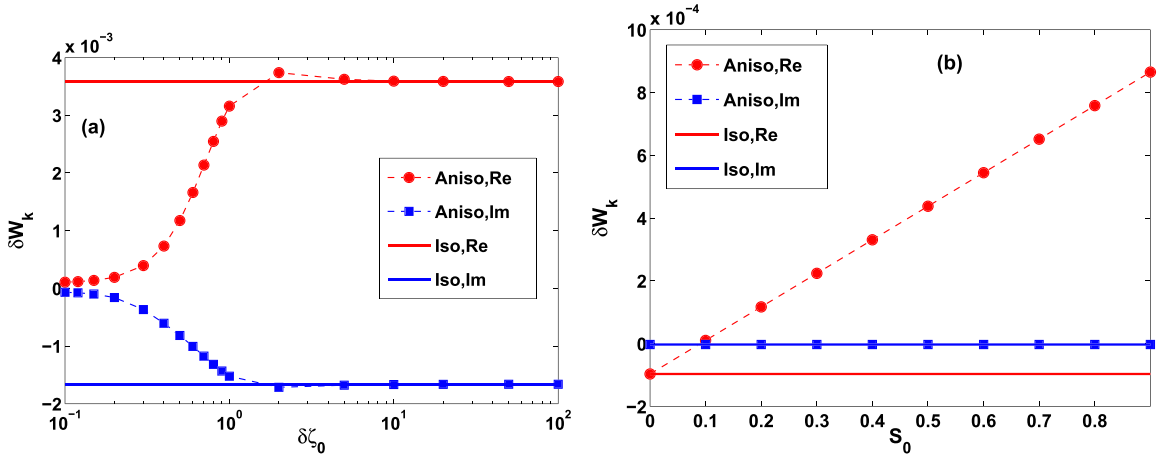

FIG. 3. Numerical recovery of isotropic results (solid lines), in terms of the perturbed drift kinetic energy computed by MARS-K, from anisotropic EP models (lines with dots), for (a) the NBI model, and (b) the ICRH model. The precessional drift resonance of trapped EPs is considered for case (a), and the transit resonance of passing EPs, with ZOW approximation, is considered for case (b).

of $\delta\zeta_0 \to \infty$, we recover δW_k, both real and imaginary parts, of the isotropic model that has been implemented in the previous version of MARS-K.[49] Similarly, by setting $\nu_T(\psi) = 1$ and a sufficiently large value of h_c in the ICRH model (8), MARS-K is able to recover δW_k of the isotropic, Maxwellian model, as the asymmetry parameter for passing particles $S_0(\psi) = S_0$ vanishes. These convergence studies verify the MARS-K implementation of the anisotropic EP models. We mention that these computations are performed for an ITER plasma, which we shall proceed to describe in Sec. IV.

We also mention a useful benchmark case for the adiabatic contributions due to EPs. For a generic anisotropic equilibrium distribution, the adiabatic parts of the perturbed kinetic pressures have to be evaluated following numerical integration of the corresponding kinetic integrals in the particle phase space. However, there are special cases where these kinetic integrals in the particle phase space can be analytically carried out. For example, if the equilibrium distribution is a Maxwellian (MARS-K allows the EPs distribution to be specified as a Maxwellian too), the adiabatic parts of the perturbed pressures, in the ZOW limit, exactly recover the fluid convection term $p^a_{||} = p^a_{\perp} = -(\xi \cdot \nabla P_j)$. For an isotropic slowing down distribution, one can show that the convective term is also recovered, but with an extra term for both $p^a_{||}$ and $p^a_{\perp}$

$$\frac{8}{15\sqrt{\pi}}\left(\frac{2\pi}{M}\right)^{3/2}\frac{d\varepsilon_a^{5/2}}{d\psi}f^0(\psi,\varepsilon_a)(\xi\cdot\nabla\psi), \qquad (44)$$

where $\varepsilon_a(\psi)$ is the particle birth energy. The above extra term is usually small, and obviously vanishes if the particle birth energy is infinity (such as for the Maxwellian) or happens to be a constant along the minor radius. For these special cases, MARS-K implements both the fluid version and the full kinetic version (with numerical integrations in the particle phase space) for computing the adiabatic parts of the perturbed pressure tensor. Systematic tests show that both versions give the same results.

Finally, we remark that MARS-K is implemented in a way that both the perturbative and the non-perturbative approaches share the same portions of code for the final system matrices, at the discrete numerical level. Therefore, a successful benchmarking of the perturbative approach also validates all the key components of the non-perturbative formulation.

IV. STABILITY OF KINETIC RWM IN ITER

In this work, we do not aim at a comprehensive prediction of the RWM stability in ITER plasmas, but rather use the ITER equilibria as an example, to show how various EPs models affect the RWM stability, according to both the perturbative and non-perturbative approaches in MARS-K.

A. ITER equilibria

We consider the 9MA steady state ITER scenario.[42] The target plasma has a normalized beta value of $\beta_N = 2.94$. For the purpose of a systematic investigation, we shall scan β_N from the no-wall limit, of 2.55, for the $n = 1$ ideal kink mode, up to the ideal-wall limit of 3.55, by varying the amplitude of the plasma pressure while keeping the pressure profile unchanged. The edge q value is also fixed at $q_a = 7.14$, which is the value for the target plasma (the plasma boundary is slightly smoothed near the X-point). This ensures a minor modification of the total plasma current while scanning the plasma pressure. Figure 4 shows radial profiles of the key equilibrium quantities, for three equilibria corresponding to $\beta_N = 2.65, 2.94, 3.65$, respectively. Note a very small modification of the q-profile while scanning the equilibrium pressure. The minimal value of q is about $q_{\min} = 1.58$. We mention that an earlier ITER design of the 9MA plasmas, for which we performed the kinetic RWM study with an isotropic EPs model and zero orbit width approximation,[41] had a rather different q-profile, with $q_{\min} = 2.3$. The toroidal rotation profile shown in Fig. 4(d) was obtained by the ASTRA simulation.[43]

Figure 5 plots the density and pressure fractions of the fusion born α's, again obtained by ASTRA. These EPs occupy about 1% of the total fuel density at the plasma core, but contribute to about 20% of the thermal pressure close to

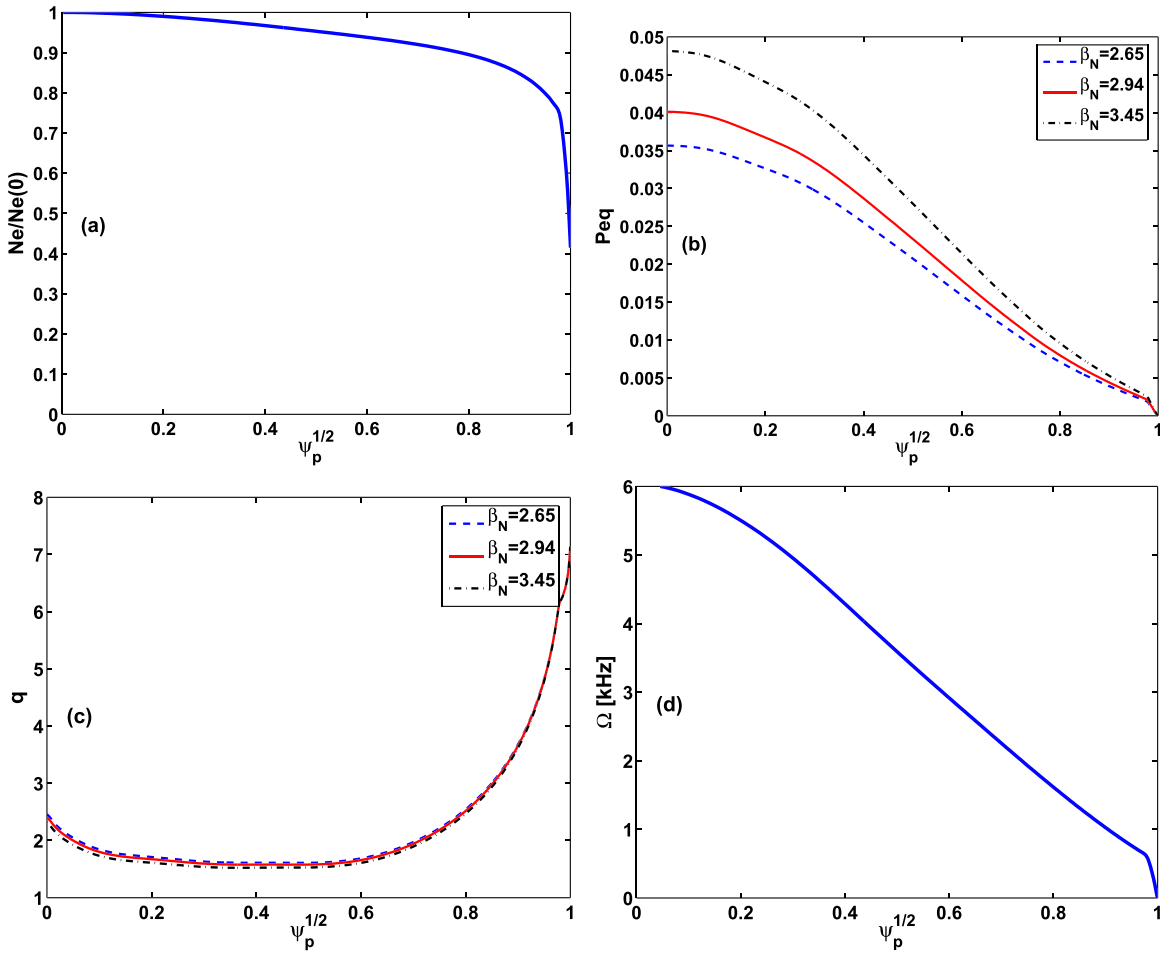

FIG. 4. The radial profiles of the equilibrium quantities for the ITER plasmas, for (a) the thermal electron density, normalized to unity at the magnetic axis; (b) the equilibrium pressure normalized by B_0^2/μ_0, for $\beta_N = 2.65, 2.94, 3.65$; (c) the safety factor q for $\beta_N = 2.65, 2.94, 3.65$; and (d) the toroidal rotation frequency.

the core. In this work, we shall use these two radial profiles as the basis to study various anisotropy and FOW effects. Understandably, a more accurate prediction of the EPs effects, induced by other sources (e.g., NNBI), requires the knowledge of the corresponding equilibrium distribution functions. On the other hand, by fixing the density and pressure profiles as the input to various EP models, we can easily assess how different equilibrium distribution models of EPs affect the stability of the RWM.

B. Results with perturbative approach

In this section, we report MARS-K results following the perturbative approach, based on the above ITER equilibria.

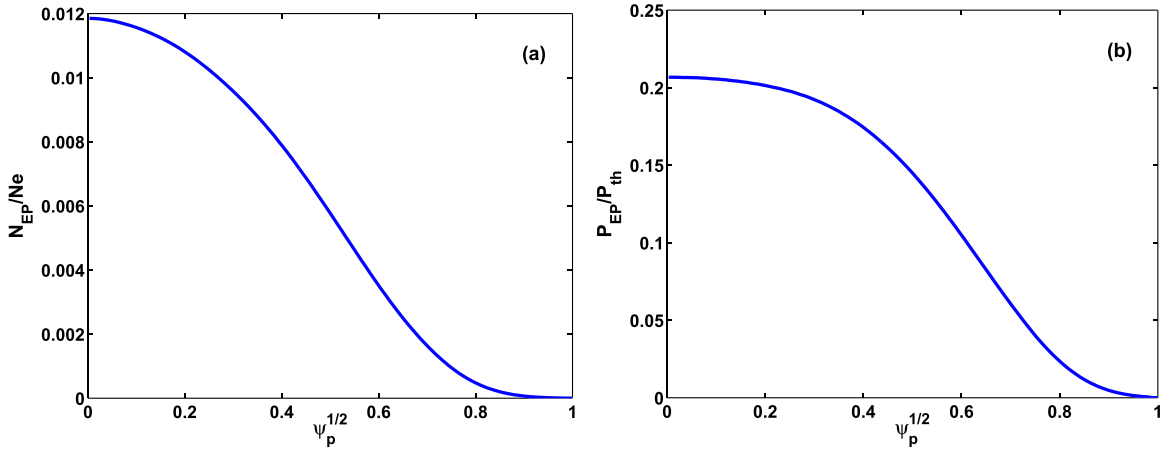

FIG. 5. The radial profiles of (a) the density and (b) the equilibrium pressure fractions for the fusion born α's obtained by the ASTRA prediction.

We use the eigenfunction of the fluid RWM as the perturbations in the drift kinetic computations. We shall mainly focus on the effects of anisotropy and FOW. The results with isotropic EPs distribution, and with the vanishing orbit width approximation, will be reported only for the purpose of comparison.

In a series of figures shown below, we shall plot and compare the perturbed drift kinetic potential energies, contributed by EPs under various assumptions, in five different components, namely the adiabatic contribution from passing particles (AP), the adiabatic contribution from trapped particles (AT), the non-adiabatic contribution from transit resonances of passing particles (NP), the non-adiabatic contribution from bounce resonances of trapped particles (NTB), and finally the non-adiabatic contribution from the toroidal precession drift resonance of trapped particles (NTD). The net drift kinetic contribution from the EPs is the sum of all these five components. All the perturbed drift kinetic energies δW_k are normalized by the inertia associated with the radial plasma displacement.

We first clarify the consequence of the two approaches, the so called $\tilde{\psi}$- and $\hat{\psi}$-approach as described in Sec. II C, on the first order FOW correction to drift kinetic results. Figure 6 shows one example of the comparison for the ITER target plasma (with $\beta_N = 2.94$). An isotropic slowing down EPs model is considered, for which the first order FOW correction vanishes for all the adiabatic contributions as well as the precessional drift resonance contribution of trapped particles, as discussed in Sec. II and confirmed here by this figure. The first order FOW remains finite for the transit and bounce resonances. The trapped particle contribution does not depend on the choice of the $\tilde{\psi}$- or $\hat{\psi}$-approach. On the other hand, these two approaches result in rather different values for the real part of the drift kinetic energy, for the transit resonance contribution from passing EPs. In fact, the $\tilde{\psi}$-approach gives an order of magnitude larger $\mathrm{Re}[\delta W_k]$ than that of the $\hat{\psi}$-approach. A detailed investigation of the numerical results reveals that all the terms in Eq. (22) are small (by an order of magnitude), compared to the two terms associated $\tilde{I}^{(1)}$ and $I^{(2)}$. These two large terms cancel well for the $\hat{\psi}$-approach, according to Eq. (33). But the cancellation does not occur for the $\tilde{\psi}$-approach, resulting in a large value of $\mathrm{Re}[\delta W_k]$ as shown in the figure. In the neoclassical theory for the bootstrap calculations due to EPs, this type of cancellation appears to be important.[35] Indeed, for the value of ψ_0 obtained in Ref. 35, the fast ion current collapses to the fast ion bootstrap current.[38] But for $\psi_0 = 0$, very large currents are produced, which are apparently unphysical. Further on, we shall only show the numerical results following the $\hat{\psi}$ approach for the first order FOW correction of passing particles. This yields a rather moderate correction to the ZOW results for EPs with isotropic equilibrium distribution. We point out that this choice is also supported by the benchmark results shown in Fig. 2, where the $\hat{\psi}$-approach is followed in the MARS-K computations. For asymmetric distributions, the FOW corrections can be more significant, as shown next.

The $\hat{\psi}$ approach also results in moderate FOW correction to the transit resonance contribution for all other EPs models that we have considered in this work, including the one shown in Fig. 7, where the kinetic contributions, again for all five components, between the isotropic model and the co-tangential NBI model, are compared. It is interesting to notice a larger FOW correction to the adiabatic contribution (AP) from the co-NBI induced passing particles. This is largely due to the asymmetric distribution of passing particles in the pitch angle space, as shown in Fig. 1 (as one example). Comparing the two EPs models considered in Fig. 7, we find that, not surprisingly, the co-tangential NBI induced EPs give much larger $|\delta W_k|$ components associated with the passing particles (both the adiabatic and the non-adiabatic contributions), than the isotropic model. [We recall that both models assume the same surface averaged density and pressure fractions for the EPs.] On the other hand, the isotropic model predicts a much larger precessional drift resonance contribution of trapped particles for this ITER plasma, than the co-NBI model. This is because the co-NBI produces a small fraction of trapped EPs. Interestingly, due to a large cancellation between the adiabatic and the non-adiabatic contributions, the net $\mathrm{Re}[\delta W_k]$ (i.e., the sum of all five components) remains the same level between the

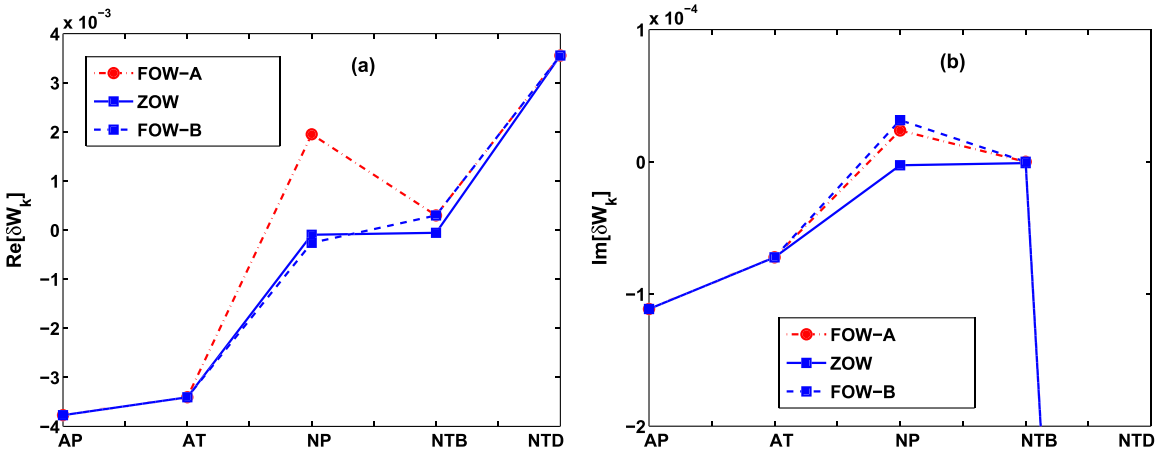

FIG. 6. The (a) real and (b) imaginary parts of the drift kinetic energy components contributed by EPs with isotropic (in particle pitch angle), slowing down (in particle energy) equilibrium distribution. Compared are cases with the ZOW approximation, with the first order FOW correction following the $\tilde{\psi}$-approach (FOW-A) and the $\hat{\psi}$-approach (FOW-B). The ITER plasma with $\beta_N = 2.94$ is considered.

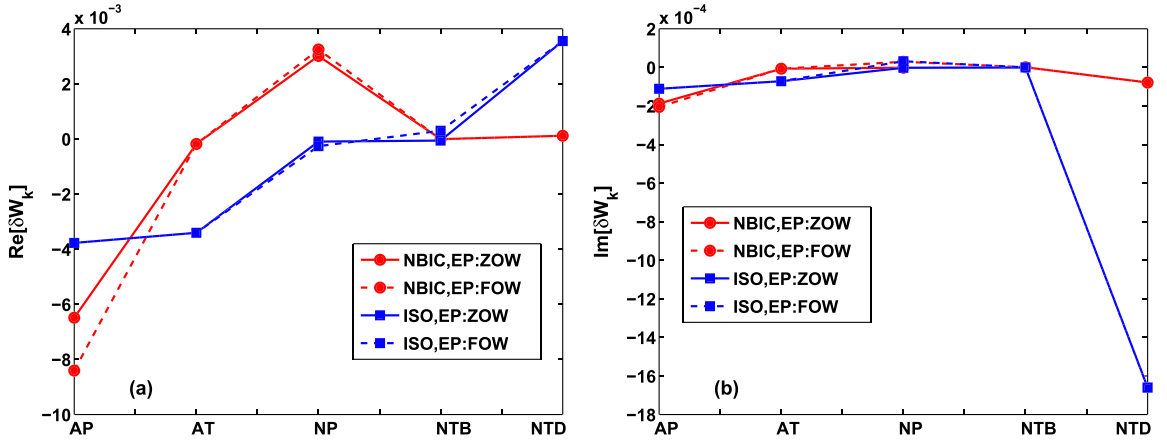

FIG. 7. The (a) real and (b) imaginary parts of the drift kinetic energy components contributed by EPs with the isotropic slowing down model (labelled "ISO") and with the co-tangential NBI model (labelled "NBIC") for the equilibrium distribution. Compared are also cases with the ZOW approximation and the first order FOW correction. The ITER plasma with $\beta_N = 2.94$ is considered.

isotropic model and the co-NBI model within the ZOW approximation. With the FOW effect, the net $\mathrm{Re}[\delta W_k]$ from the co-NBI model is about 25% larger in amplitude, than the isotropic model, largely due to the FOW correction to the adiabatic contribution by passing particles. The net $\mathrm{Im}[\delta W_k]$ from the isotropic EPs is one order of magnitude larger than the co-NBI induced EPs, due to the large precessional drift resonance contribution by the former.

Figure 8 performs similar comparisons, but between the normal and co-tangential injection angles for the NBI model. The most noticeable difference is that the normal injection introduces much higher fraction of trapped particles, and consequently, much larger δW_k (by amplitude) components from the adiabatic, as well as from the non-adiabatic bounce and precessional drift resonances of trapped EPs. Within the ZOW approximation, the large cancellation between the adiabatic contribution and the precessional drift contribution from trapped EPs, for the normal injection, results in a similar level of the net $\mathrm{Re}[\delta W_k]$ as compared to the co-NBI case (though the signs of the net $\mathrm{Re}[\delta W_k]$ are opposite). The net $\mathrm{Im}[\delta W_k]$ is much larger from the normal injection, again due to the large fraction of trapped particles resulted precessional resonance contribution. The FOW introduces a significant correction, both in the real and imaginary parts, to the bounce resonance in the normal injection case. This yields two notable effects on the net δW_k: (i) the real part is about 4 times larger in the normal injection case than in the co-NBI injection case; (ii) the imaginary parts are small for both EPs models, due to a rather good cancellation between the FOW enhanced bounce resonance contribution on one side, and the precession resonance contribution on the other side, of trapped particles.

We also consider the kinetic effects from the ICRH model introduced EPs. In this study, we choose $S_0(\psi) = const = 0.2, \nu_T(\psi) = const = 1.3$ in Eq. (8), and h_c right in the middle between the minimal and the maximal equilibrium magnetic field amplitudes inside the plasma. We again assume the same surface averaged density and pressure fractions for the ICRH driven EPs, as for the other EPs models. We emphasize that the sole purpose of these choices is to make the comparative study more meaningful. This by no means reflects the EPs distribution induced by the true ITER ICRH system. A dedicated systematic study of the kinetic RWM stability in ITER plasmas, where more realistic models of EPs, from either NBI or ICRH heating, will be carried out in a future work.

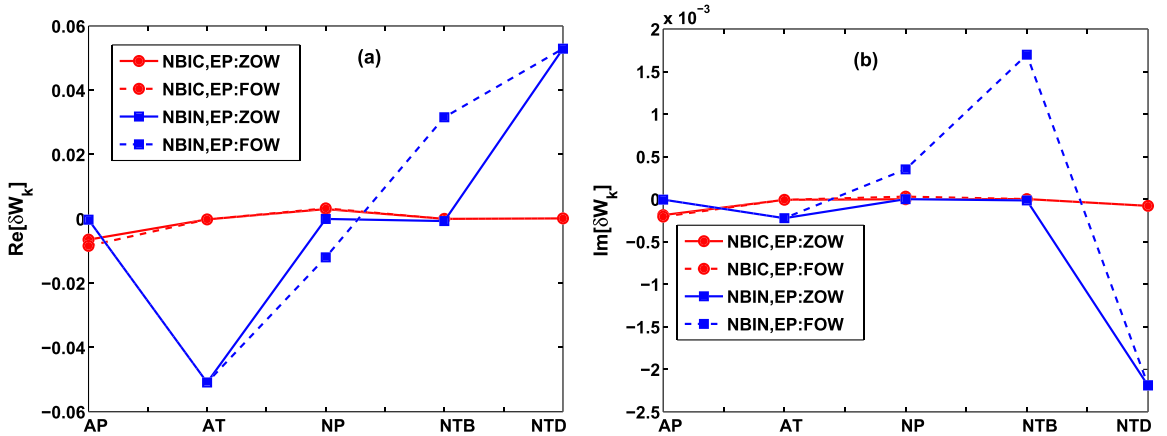

FIG. 8. The (a) real and (b) imaginary parts of the drift kinetic energy components contributed by EPs with the normal-injection NBI model (labelled "NBIN") and with the co-tangential injection NBI model (labelled "NBIC") for the equilibrium distribution. Compared are also cases with the ZOW approximation and the first order FOW correction. The ITER plasma with $\beta_N = 2.94$ is considered.

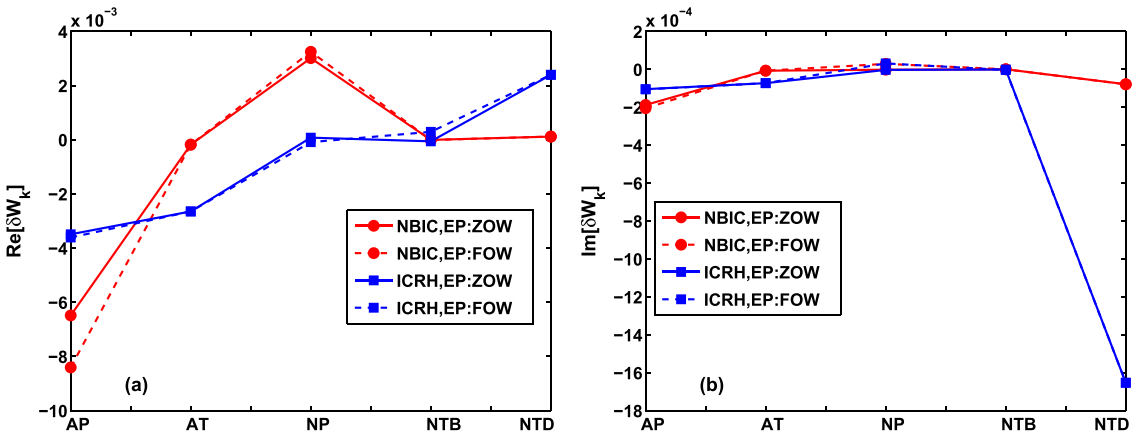

FIG. 9. The (a) real and (b) imaginary parts of the drift kinetic energy components contributed by EPs with the ICRH model (labelled "ICRH") and with the co-tangential injection NBI model (labelled "NBIC") for the equilibrium distribution. Compared are also cases with the ZOW approximation and the first order FOW correction. The ITER plasma with $\beta_N = 2.94$ is considered.

Figure 9 compares the drift kinetic energies between two EPs distributions: the co-tangential NBI model and the ICRH model. This comparison is similar to that of Fig. 7. In other words, the ICRH model, with the chosen parameters here, produces a similar drift kinetic effect as that of the isotropic slowing down EPs. We point out, however, that the asymmetry effect of the ICRH model can become much larger as we increase the value of the parameter S_0, as shown in Fig. 3(b). Also, the trapped effects can become much stronger as ν_T is increased.

The above results so far have been focusing on comparison of various EP models, and the revelation of various subtle cancellation effects. We have chosen a single plasma equilibrium (the ITER target) for this purpose. These results are helpful in understanding the next four groups of figures, Figs. 10–13, which report the perturbative results while

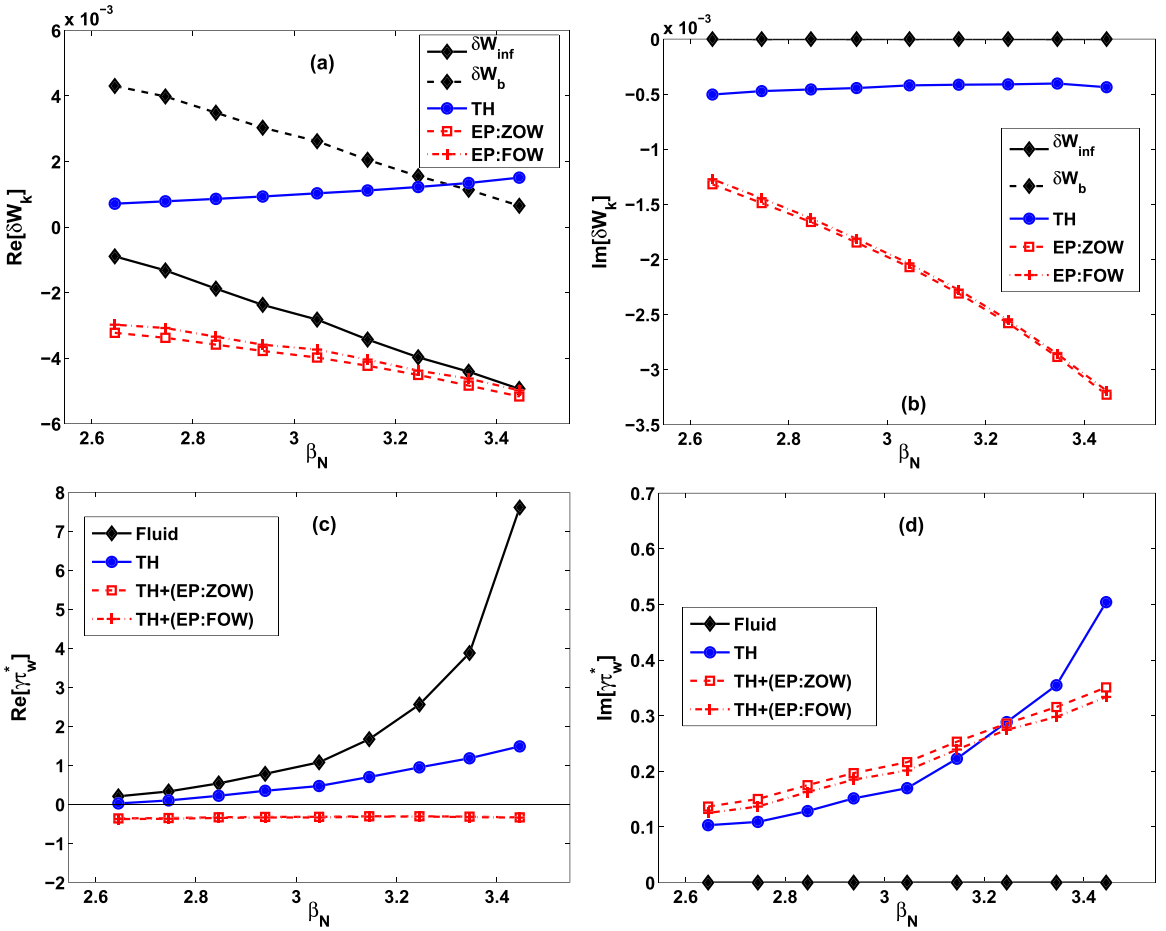

FIG. 10. Comparison of the perturbed energy components ((a) and (b)) from thermal particles, EPs with ZOW approximation, and EPs with the FOW correction. Compared are also the corresponding RWM eigenvalues ((c) and (d)) computed following the perturbative approach. Both the real ((a) and (c)) and imaginary ((b) and (d)) parts are plotted. The isotropic slowing down model is assumed for the EPs.

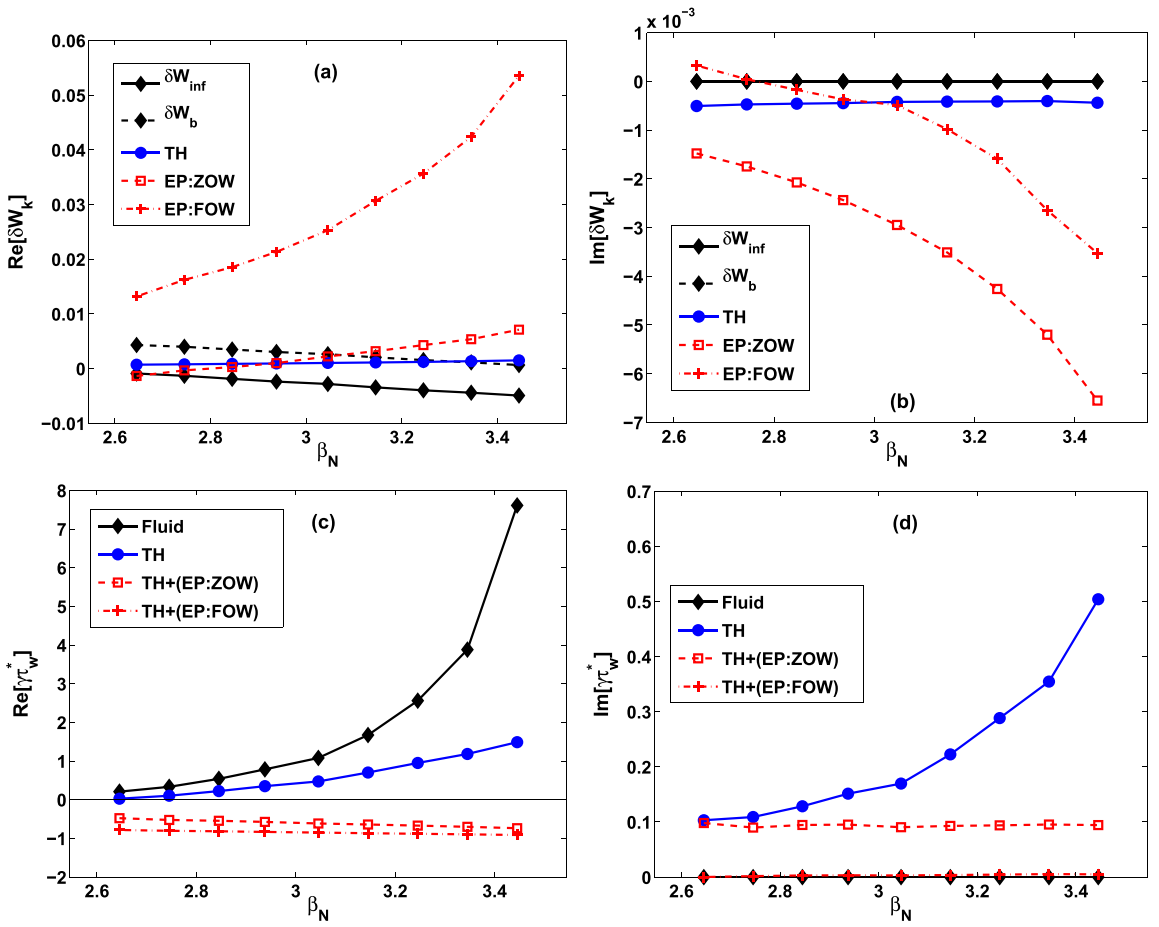

FIG. 11. Comparison of the perturbed energy components ((a) and (b)) from thermal particles, EPs with ZOW approximation, and EPs with the FOW correction. Compared are also the corresponding RWM eigenvalues ((c) and (d)) computed following the perturbative approach. Both the real ((a) and (c)) and imaginary ((b) and (d)) parts are plotted. The NBI model with normal injection angle is assumed for the EPs.

scanning the plasma pressure from the no-wall to the ideal-wall beta limits, using the four EPs models, respectively. In each group, we plot and compare the real and imaginary parts of the following energy components: the fluid potential energy $\delta W_{\rm inf}$ with wall at infinity; the fluid potential energy δW_b with an ideal wall located at the inner wall position of the ITER vacuum vessels; the net non-adiabatic drift kinetic contribution (labelled "TH"), including transit, bounce, and precessional resonances, from thermal particles (both ions and electrons); the net kinetic contribution, including both adiabatic and non-adiabatic parts with transit, bounce, and precession resonances, from EPs within the ZOW approximation (labelled "EP:ZOW") and with inclusion of the first order FOW corrections (labelled "EP:FOW"). Compared are also the corresponding eigenvalues of the kinetic RWM, computed using the following RWM dispersion relation:

$$\gamma\tau_w^* = -\frac{\delta W_{\rm inf} - \delta W_{\rm DB} + \delta W_k}{\delta W_b - \delta W_{\rm DB} + \delta W_k}, \tag{45}$$

where τ_w^* is the characteristic wall time, and δW_k is the kinetic energies described above, for thermal or EPs contributions accordingly. The additional term $\delta W_{\rm DB}$ is introduced to avoid double counting of the adiabatic contribution from EPs. As mentioned earlier, the adiabatic contribution from EPs does not generally recover the convective term in the fluid equation for the perturbed pressure. This leaves certain ambiguity in how to include the adiabatic contribution of EPs into the RWM energy principle for the perturbative approach. The fluid potential energies, $\delta W_{\rm inf}$ and δW_b, correctly include the adiabatic contributions from the thermal particles (and hence $\delta W_{\rm DB} = 0$ for thermal particles). This adiabatic portion is eventually responsible for the pressure driving term in the ideal MHD energy analysis. However, in order to correctly include the adiabatic contribution of EPs, we need to subtract a portion of pressure driving potential fluid energy, which is supposed to be replaced by the EPs contribution. This is because we assume that the equilibrium pressure includes both thermal and energetic particle pressures. Therefore, for EPs, we first compute $\delta W_{\rm DB}$ as the difference between the (total) fluid pressure driven energy, and the adiabatic contribution of thermal particles. We then add the net δW_k of EPs including both adiabatic and non-adiabatic contributions.

We point out that for the non-perturbative approach, there is no such an ambiguity issue, since the equation of state from the standard single fluid formulation is completely replaced by the drift kinetic solution for the perturbed pressure. On the other hand, due to an earlier mentioned caveat on the isotropic equilibrium solution used in our formulation,

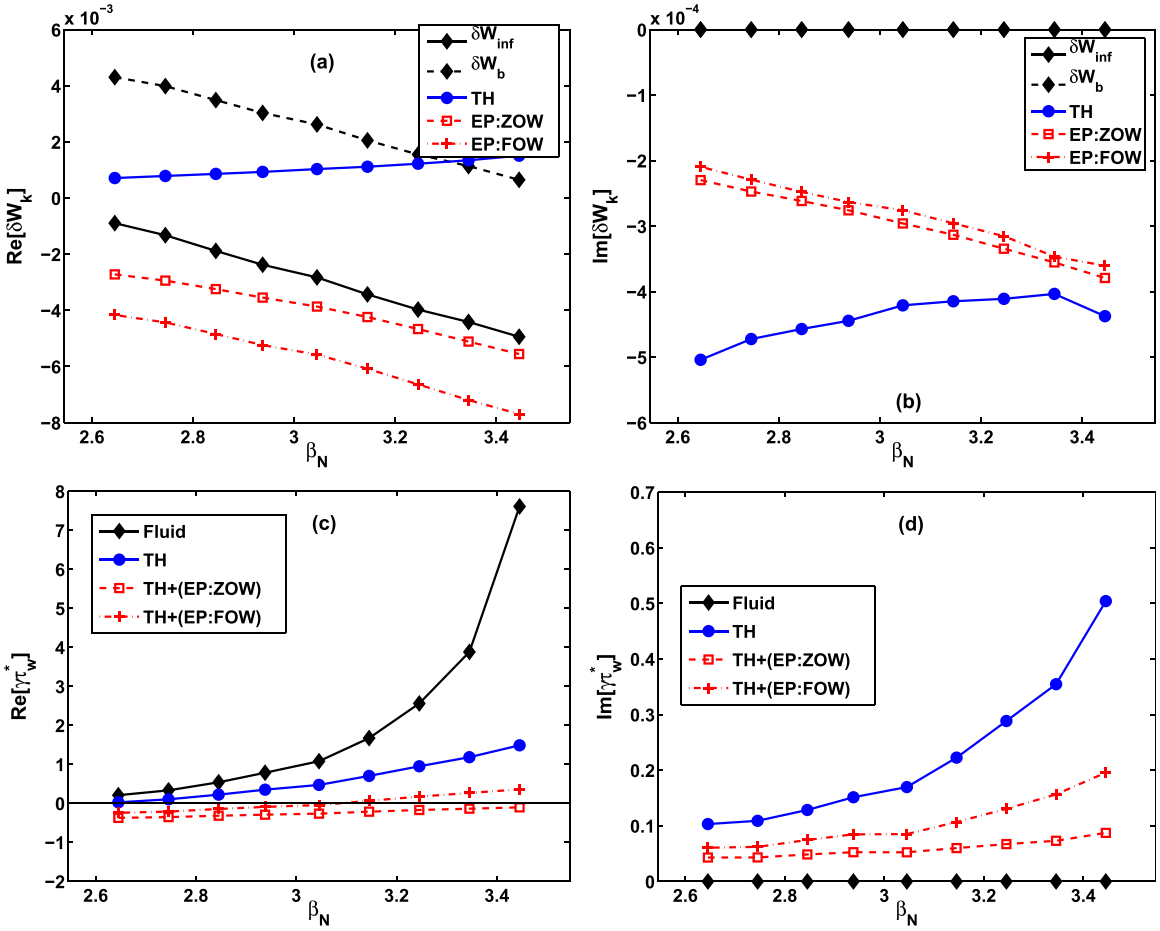

FIG. 12. Comparison of the perturbed energy components ((a) and (b)) from thermal particles, EPs with ZOW approximation, and EPs with the FOW correction. Compared are also the corresponding RWM eigenvalues ((c) and (d)) computed following the perturbative approach. Both the real ((a) and (c)) and imaginary ((b) and (d)) parts are plotted. The NBI model with co-tangential injection angle is assumed for the EPs.

the above statement only holds when the anisotropic equilibrium pressure fraction is sufficiently low.

Now we proceed to describing the detailed results shown in Figs. 10–13, for each EPs model, respectively. Figure 10 reports results by assuming an isotropic slowing down equilibrium distribution for EPs. The perturbed fluid potential energy is always negative (destabilizing) without wall and positive (stabilizing) with an ideal wall. This corresponds to the fluid-wise unstable RWM regime.

The kinetic effects from thermal particles alone greatly reduce the growth rate of the RWM in ITER, but do not yield a significant increase of the stability margin. This quantitatively agrees well with the HAGIS prediction,[15] where the same ITER equilibria were used, and qualitatively agrees with an earlier ITER simulation,[41] where an earlier version of the ITER 9MA design was used. We also mention that only the precessional drift resonance contribution of trapped particles was included in the computations performed in Ref. 41. The kinetic results from thermal particles, reported here in Fig. 10, remain the same while changing the EPs models, by virtue of keeping the same density and pressure fractions for all EPs models.

Inclusion of the EPs contribution significantly changes the stability of the RWM. In fact, the mode is fully stabilized for all plasma pressures (up to the ideal wall limit), following the perturbative prediction. This prediction is more optimistic than the HAGIS results,[15] possibly due to the fact that the HAGIS simulations include the adiabatic contributions from EPs, without subtraction of the corresponding portion from the fluid potential energy. We emphasize again that, generally speaking, this subtraction cannot be rigorously performed in the perturbative approach. Other possible reasons for this discrepancy may come from the fact that HAGIS performs full orbit computations from EPs, whilst MARS-K only keeps the first order correction. For the isotropic EPs model, it appears that the first order correction gives a very minor effect on the mode stability. The strong stabilizing effect of the isotropic EPs on the RWM (within the perturbative approach) confirms an earlier finding,[41] despite the difference in the assumed equilibria.

Figure 11 reports the perturbative results by assuming the EPs model with normal NBI injection. As already noticed earlier, the FOW correction yields a significant modification to the perturbed kinetic energy (mainly due to the contribution from bounce resonance of trapped EPs). However, the net effect is again a full stabilization of the mode up to the ideal wall beta limit, when the kinetic effects of EPs are included, either in the ZOW or the first order FOW approximation.

The predictions are different with the co-injection NBI model for the EPs, as shown in Fig. 12. In this case, the

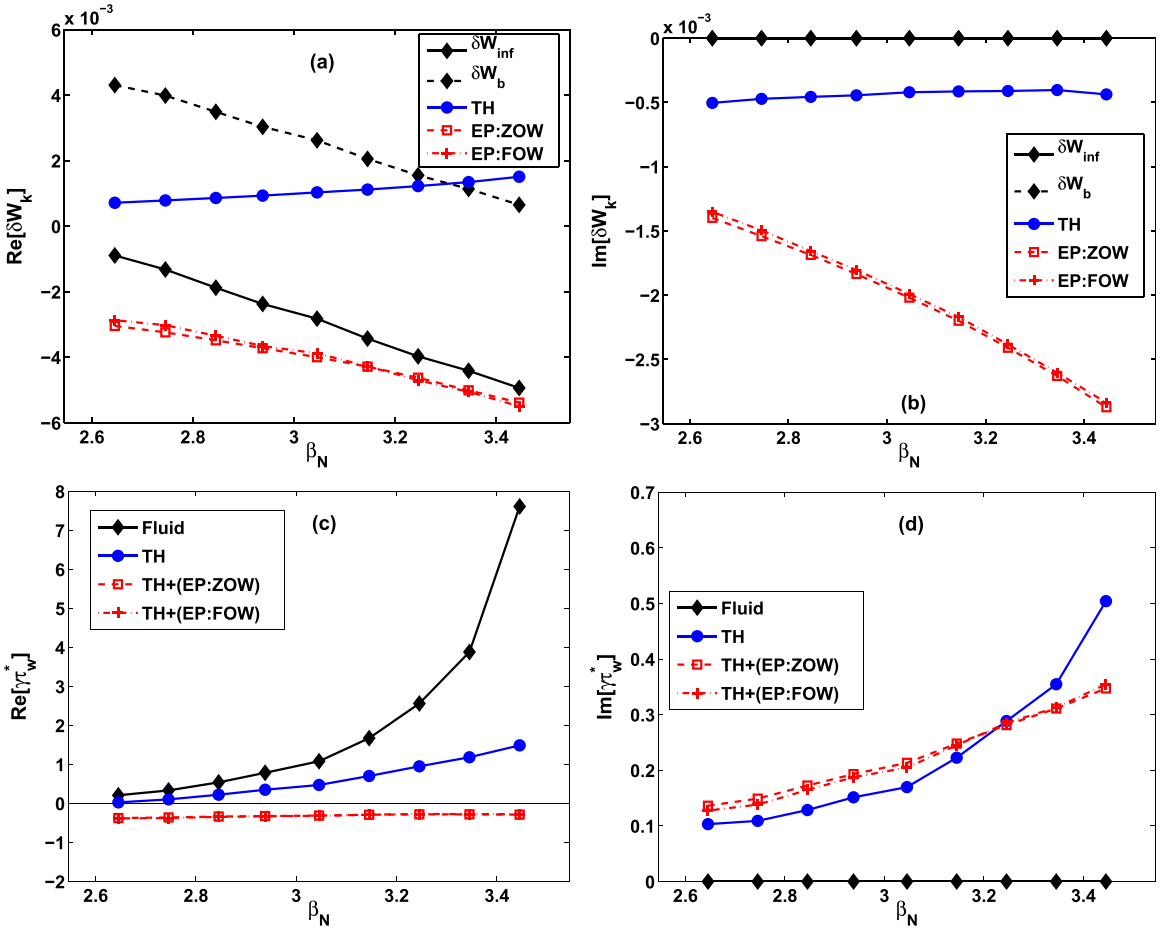

FIG. 13. Comparison of the perturbed energy components ((a) and (b)) from thermal particles, EPs with ZOW approximation, and EPs with the FOW correction. Compared are also the corresponding RWM eigenvalues ((c) and (d)) computed following the perturbative approach. Both the real ((a) and (c)) and imaginary ((b) and (d)) parts are plotted. The ICRH model is assumed for the EPs.

ZOW approximation still predicts a (nearly) fully stabilization of the mode up to the ideal beta limit. However, with the FOW correction, only partial stabilization is predicted, with the marginal point shifted roughly in the middle between the no-wall and the ideal-wall beta limits. The remaining instability becomes rather weak though. The major contribution of the FOW destabilisation comes from the adiabatic contribution of passing particles in this case.

The ICRH model of EPs yields similar kinetic results (Fig. 13) for the RWM stability, to that of the isotropic slowing down model. As pointed out before, this is possibly because of the choice of parameters in the ICRH model, which gives a weak anisotropy/asymmetry of the particle equilibrium distribution.

C. Results with non-perturbative approach

Now we report the RWM stability, predicted by non-perturbative MARS-K computations for these ITER equilibria. We again focus on the comparison of the two major aspects in this work: isotropic versus anisotropic models for EPs, and the ZOW approximation versus the FOW correction. We shall consider only two EP models, i.e., the isotropic slowing down model and the co-tangential NBI model. The former should reasonably well describe the fusion born α's, whilst the later corresponds to the NNBI system designed for ITER.[33]

Figure 14 summarizes the modelling results with the isotropic EP model. We compare the growth rates, as well as the real mode frequencies, predicted by the fluid theory and the drift kinetic theory with three different assumptions. In the first case (diamonds), we include only the precession resonances of all particle species (both thermal ion, electrons, and energetic). In the second case (squares), we include the precession resonance of thermal electrons, as well as the bounce and transit resonances for thermal ions and EPs (the bounce and transit resonance contributions from thermal electrons are small). All the resonances assume the ZOW approximation. The third case (crosses) differs from the second by the addition of FOW corrections to the bounce and transit resonance contributions, as well as to the adiabatic contributions, from EPs. Overall, the drift kinetic theory predicts a much slower growth of the mode than the fluid theory, thanks to the kinetic damping effects. The strongest damping comes from the precessional drift resonances of both thermal and energetic particles. The inclusion of this resonance alone would predict a stability margin of $\beta_N \simeq 3$ for this ITER design. This is qualitatively similar, but somewhat more optimistic than the prediction for an earlier ITER design.[41] In both cases, however, the

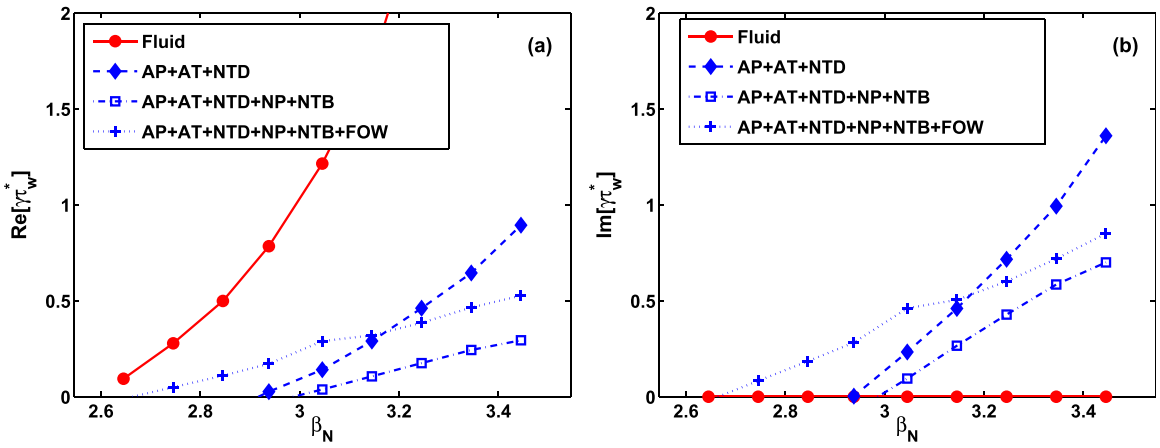

FIG. 14. Comparison of the (a) real and (b) imaginary parts of the RWM eigenvalues in ITER, computed by MARS-K assuming the fluid model (closed circles), the kinetic model with precessional drift resonances (closed diamonds), the kinetic model with all drift resonances at ZOW approximation (open squares), and the kinetic model with all drift resonances and FOW correction (crosses). The isotropic slowing down equilibrium distribution is assumed for EPs.

non-perturbative approach predicts less kinetic stabilization, than the perturbative approach.

The bounce and transit resonance contributions (from both thermal ions and EPs), within the ZOW approximation, slightly destabilize the RWM, shifting the marginal stability point slightly below $\beta_N = 3$ (close to the ITER target value). The inclusion of the FOW corrections for EPs yields some degree of destabilization of the mode, effectively further reducing the marginal stability point. We point out though that since the growth rates of these kinetic RWMs are rather small, any additional damping effects may fully stabilize the mode. One example is the parallel sound wave damping model,[29,31] which we neglected in these non-perturbative computations. We find that adding a rather small parallel sound wave damping (which may be physically meaningful in the context of the subsonic flow assumption made in our hybrid formulation) can fully damp these weakly unstable RWMs. Even without additional damping, a weakly unstable RWM can be relatively easily controlled by a magnetic feedback scheme.[44–47] On the other hand, depending on the plasma parameters (rotation, EPs pressure fraction, etc.), there can be more than one branch of unstable modes.[8,41] One instability, referred to as the fishbone-like mode,[8] can occur purely due to the energetic particle drive. In this study, we focus only on the kinetic RWM branch.

Compared with the isotropic model, less kinetic stabilization of the mode is obtained with the co-tangential NBI induced EPs, as shown in Fig. 15. This qualitatively agrees with the comparative results based on the perturbative approach. On the other hand, the bounce and transit resonance contributions from EPs are slightly stabilizing. The FOW corrections do not yield a noticeable change of the mode stability compared to the ZOW results, for this co-tangential NBI model, even though the perturbative approach shows slightly stronger FOW correction effect. This seems to indicate that FOW corrections are more effective for trapped particles. A more clear confirmation of this is shown in the perturbative results, Fig. 8, where the normal NBI produces predominantly trapped particles.

For the ITER equilibria considered in this work, the RWM eigenfunction is modified by the drift kinetic effects. Figure 16 shows two examples. Figures 16(a) and 16(c) compare the fluid RWM eigenfunction, in terms of the dominant poloidal Fourier harmonics of the perturbed radial velocity,

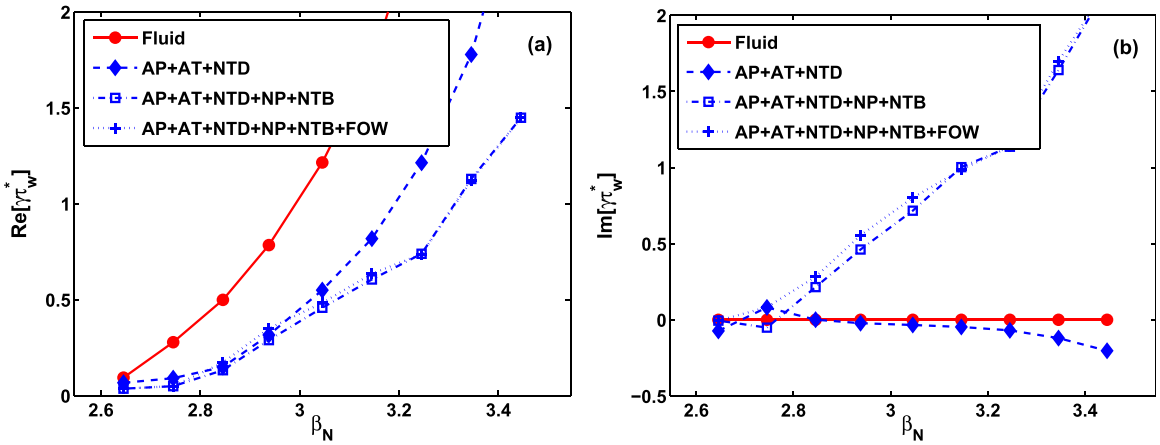

FIG. 15. Comparison of the (a) real and (b) imaginary parts of the RWM eigenvalues in ITER, computed by MARS-K assuming the fluid model (closed circles), the kinetic model with precessional drift resonances (closed diamonds), the kinetic model with all drift resonances at ZOW approximation (open squares), and the kinetic model with all drift resonances and FOW correction (crosses). The co-tangential NBI model is assumed for EPs.

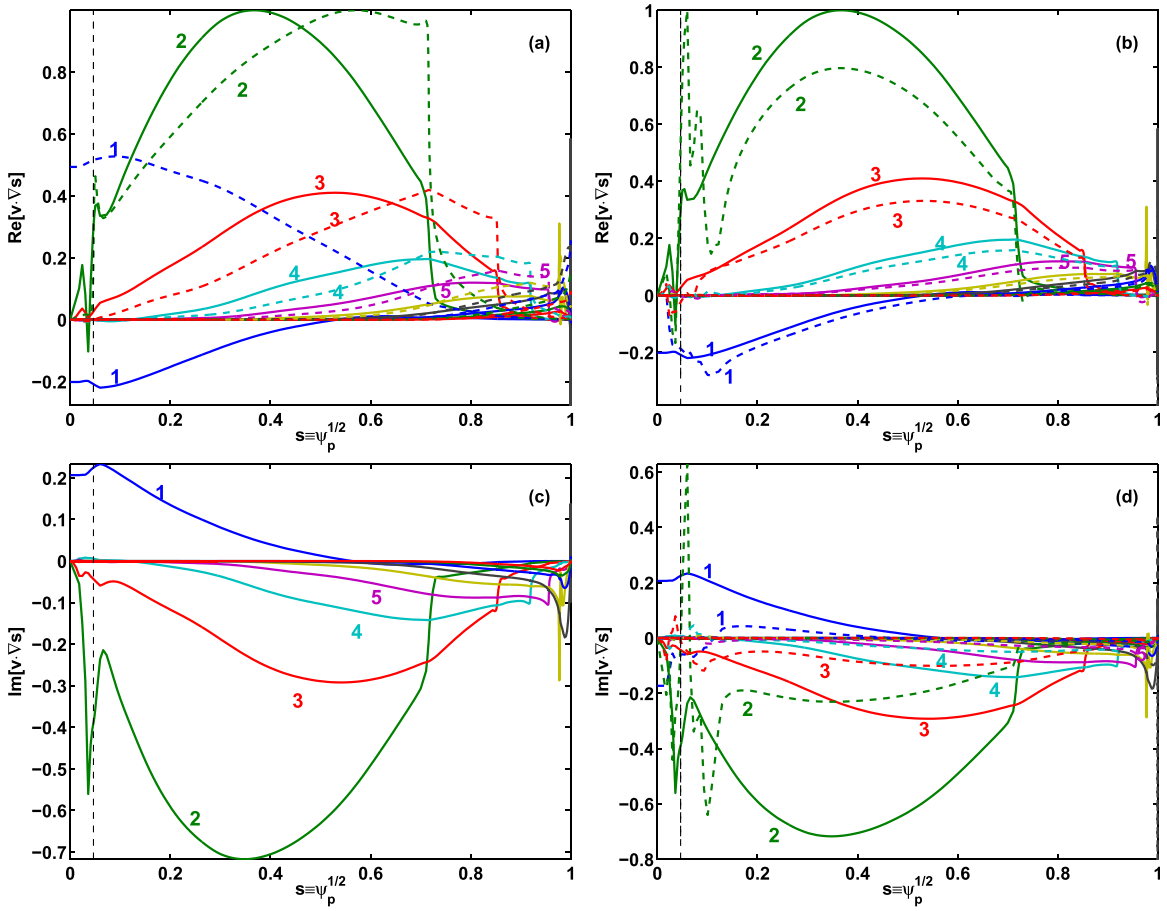

FIG. 16. Comparison of eigenfunctions of the RWM ((a) and (c)) between fluid theory (solid) and the full drift kinetic theory at ZOW approximation (dashed), and ((b) and (d)) between the ZOW (solid) and first order FOW (dashed) approximations, for dominant poloidal Fourier harmonics of the perturbed radial displacement, for the ITER equilibrium with $\beta_N = 3.05$. Both the real ((a) and (b)) and the imaginary ((c) and (d)) parts of the eigenfunctions are compared, with a toroidal phase chosen such that the imaginary part for the fluid RWM eigenfunction vanishes. An isotropic slowing down model is assumed for the EPs. The vertical dashed lines indicate the location of the inner $q = 2$ rational surface. The Fourier harmonics are decomposed in a straight field line coordinate system.

with that obtained from the non-perturbative computations, where the full kinetic resonance effects (precession, bounce, and transit) are included for both thermal and energetic particles, with the latter considered in the ZOW approximation. We notice a rather global modification of the radial velocity for the $m = 1, 2, 3, 4$ harmonics. In particular, the $m = 1$ harmonic changes sign. Note that since the toroidal plasma rotation is also self-consistently included into the non-perturbative computations, the eigenfunction is partially modified by the plasma flow. In the perturbative computations, the toroidal flow of the plasma is neglected in computing the fluid RWM eigenfunction. Figures 16(b) and 16(d) compare the kinetic RWM eigenfunctions with and without the FOW correction. Here, again the full drift kinetic resonances from both thermal and energetic particles are included in the non-perturbative computations. The FOW effect leads to additional modifications of the mode's eigenfunction, mostly in the plasma core region. In fact, when the amplitude of the Fourier harmonics is plotted and compared, it appears that most of the modification due to the FOW effect occurs near or inside the inner $q = 2$ surface. The somewhat larger difference outside the inner $q = 2$ surface, as shown in Figs. 16(b) and 16(d), is due to the additional toroidal phase shift introduced by the FOW effect. This seems to indicate that the transit resonance of passing EPs is playing a dominant role in this FOW induced eigenfunction modification. This additional correction to the mode's eigenfunction is not due to the numerical truncation of the FOW terms near the inner $q = 2$ rational surface, since this truncation is applied to all the other rational surfaces too.

V. CONCLUSION AND DISCUSSION

A MHD-kinetic hybrid formulation is presented in this work that includes two major improvements towards realistic modelling of the kinetic effects of energetic particles on the RWM stability. The anisotropy, as well as asymmetry,[20] of the equilibrium distribution of EPs, along the particle pitch angle, affects both the adiabatic and non-adiabatic contributions to the perturbed drift kinetic energy associated with the RWM. A non-perturbative formulation is developed for the first order FOW corrections to the EPs kinetic contribution, based on rigorous assumptions and derivations.[35] The first order FOW correction vanishes for the adiabatic contribution of trapped particles, as well as the passing particles if the latter has a symmetric equilibrium distribution along the particle pitch angle. The correction also vanishes for the precessional drift resonance contribution of trapped particles.

However, the correction remains finite for the non-adiabatic contributions due to transit or bounce resonances.

An interesting theoretical aspect of this FOW formulation is that the final expressions for the perturbed drift kinetic pressure tensor depend on the choice of specifications of the equilibrium distribution function. Both the benchmark result with the HAGIS code and the numerical results for the ITER plasmas seem to suggest that a prescription following the neoclassical theory (for bootstrap current calculations) represents the more physical choice.

The hybrid formulation has been implemented in MARS-K, and successfully benchmarked against the full orbit particle guiding centre following code HAGIS. MARS-K is then applied to study the RWM stability for a series of ITER equilibria, with the main focus being on comparisons between the isotropic and anisotropic effects, as well as between the ZOW approximation and FOW corrections. Numerical results, from both perturbative and non-perturbative approaches, confirm that both effects can be important for realistic prediction of the RWM stability in ITER plasmas. In particular, the anisotropy effects cannot be neglected for the NBI induced or ICRH wave resonance induced EPs, though in certain cases, interesting cancellations occur (e.g., between the anisotropy induced adiabatic contribution and the anisotropy induced non-adiabatic contribution).[48] The FOW correction is found to be important for non-perturbative modelling of the isotropic EPs (fusion born α's), but less important for EPs from co-tangential NBI. Comparing the results from the perturbative versus the non-perturbative approaches, we find that the latter always predicts less stabilisation of the RWM than the former. This re-affirms our earlier conclusion,[41] which was only based on the isotropic model and with the ZOW assumption for EPs. Finally, the non-perturbative computations confirm that, for the ITER plasmas considered in this work, the drift kinetic effects modify the eigenfunction of the RWM.

We point out that this work does not cover a comprehensive modelling of the ITER plasmas. In particular, a more realistic prediction requires accurate input data for the energetic particle distributions (or at least the surface averaged radial density and pressure distributions of EPs), which are consistent with the NBI and ICRH systems in the ITER design.

Further improvement of the present hybrid formulation is possible, and may be necessary. For instance, the inclusion of the perturbed electrostatic potential, which is currently neglected for the RWM study. The present formulation always assumes that the trapped particles are symmetrically distributed with respect to the parallel velocity, which may not always be the case, in particular, in present day tokamaks. Moreover, the present formulation requires that the EP pressure is small, or the anisotropy is weak when pressure is large, so that an isotropic equilibrium can be assumed.

ACKNOWLEDGMENTS

This work was part-funded by the RCUK Energy Programme under Grant No. EP/I501045 and the European Communities under the contract of Association between EURATOM and CCFE. To obtain further information on the data and models underlying this paper, please contact PublicationsManager@ccfe.ac.uk. The views and opinions expressed herein do not necessarily reflect those of the European Commission. G.Z.H. would like to acknowledge the support from the National Natural Science Foundation of China under No. 11205051 and the National Magnetic Confinement Fusion Science Program of China under No. 2014GB124004.

[1]T. C. Hender, J. C. Wesley, J. Bialek, A. Bondeson, A. H. Boozer, R. J. Buttery, A. Garofalo, T. P. Goodman, R. S. Granetz, Y. Gribov, O. Gruber, M. Gryaznevich, G. Giruzzi, S. Guenter, N. Hayashi, P. Helander, C. C. Hegna, D. F. Howell, D. A. Humphreys, G. T. A. Huysmans, A. W. Hyatt, A. Isayama, S. C. Jardin, Y. Kawano, A. Kellman, C. Kessel, H. R. Koslowski, R. J. La Haye, E. Lazzaro, Y. Q. Liu, V. Lukash, J. Manickam, S. Medvedev, V. Mertens, S. V. Mirnov, Y. Nakamura, G. Navratil, M. Okabayashi, T. Ozeki, R. Paccagnella, G. Pautasso, F. Porcelli, V. D. Pustovitov, V. Riccardo, M. Sato, O. Sauter, M. J. Schaffer, M. Shimada, P. Sonato, E. J. Strait, M. Sugihara, M. Takechi, A. D. Turnbull, E. Westerhof, D. G. Whyte, R. Yoshino, H. Zohm, and the ITPA MHD, Disruption and Magnetic Control Topical Group, Nucl. Fusion **47**, S128 (2007).
[2]F. Troyon, R. Gruber, H. Saurenmann, S. Semenzato, and S. Succi, Plasma Phys. Controlled Fusion **26**, 209 (1984).
[3]M. S. Chu and M. Okabayashi, Plasma Phys. Controlled Fusion **52**, 123001 (2010).
[4]B. Hu and R. Betti, Phys. Rev. Lett. **93**, 105002 (2004).
[5]A. Bondeson and D. J. Ward, Phys. Rev. Lett. **72**, 2709 (1994).
[6]R. Betti, Phys. Rev. Lett. **74**, 2949 (1995).
[7]Y. Liu, M. S. Chu, C. G. Gimblett, and R. J. Hastie, Phys. Plasmas **15**, 092505 (2008).
[8]G. Z. Hao, A. K. Wang, Y. Q. Liu, and X. M. Qiu, Phys. Rev. Lett. **107**, 015001 (2011).
[9]G. Z. Hao, Y. Q. Liu, A. K. Wang, H. B. Jiang, G. Lu, H. D. He, and X. M. Qiu, Phys. Plasmas **18**, 032513 (2011).
[10]Y. Q. Liu, M. S. Chu, I. T. Chapman, and T. C. Hender, Phys. Plasmas **15**, 112503 (2008).
[11]I. T. Chapman, M. P. Gryaznevich, C. G. Gimblett, T. C. Hender, D. F. Howell, Y. Q. Liu, S. D. Pinches, and JETEFDA Contributors, Plasma Phys. Controlled Fusion **51**, 055015 (2009).
[12]Y. Liu, M. S. Chu, I. T. Chapman, and T. C. Hender, Nucl. Fusion **49**, 035004 (2009).
[13]J. W. Berkery, S. A. Sabbagh, H. Reimerdes, R. Betti, B. Hu, R. E. Bell, S. P. Gerhardt, J. Manickam, and M. Podesta, Phys. Plasmas **17**, 082504 (2010).
[14]Z. R. Wang, S. C. Guo, Y. Q. Liu, and M. S. Chu, Nucl. Fusion **52**, 063001 (2012).
[15]I. T. Chapman, Y. Q. Liu, O. Asunta, J. P. Graves, T. Johnson, and M. Jucker, Phys. Plasmas **19**, 052502 (2012).
[16]B. Hu, R. Betti, and J. Manickam, Phys. Plasmas **12**, 057301 (2005).
[17]L. J. Zheng, M. Kotschenreuther, and J. W. Van Dam, J. Comput. Phys. **229**, 3605 (2010).
[18]L. J. Zheng, M. Kotschenreuther, and J. W. Van Dam, Phys. Plasmas **17**, 056104 (2010).
[19]L. J. Zheng, M. Kotschenreuther, and J. W. Van Dam, Phys. Plasmas **14**, 072505 (2007).
[20]J. P. Graves, I. T. Chapman, S. Coda, M. Lennholm, M. Albergante, and M. Jucker, Nature Commun. **3**, 624 (2012).
[21]J. P. Graves, I. T. Chapman, S. Coda, T. Johnson, M. Lennholm, and JET-EFDA Contributors, Phys. Plasmas **17**, 056118 (2010).
[22]S. I. Braginskii, in *Review of Plasma Physics*, edited by M. A. Leontovich (Consultants Bureau, New York, 1965), Vol. 1, p. 205.
[23]A. Brizard, Phys. Fluids B **4**, 1213 (1992).
[24]J. P. Graves, R. J. Hastie, and K. I. Hopcraft, Plasma Phys. Controlled Fusion **42**, 1049 (2000).
[25]T. M. Antonsen and A. Bondeson, Phys. Fluids B **5**, 4090 (1993).
[26]L. J. Zheng, M. S. Chu, and L. Chen, Phys. Plasmas **6**, 1217 (1999).
[27]A. Bondeson and R. Iacono, Phys. Fluids B **1**, 1431 (1989).

[28]H. Grad, in *Proceedings of the Symposium on Electromagnetic and Fluid Dynamics of Gaseous Plasma* (Polytechnic Institute of Brooklyn, New York, 1961), p. 37.
[29]D. J. Ward and A. Bondeson, Phys. Plasmas **2**, 1570 (1995).
[30]D. Gregoratto, A. Bondeson, M. S. Chu, and A. M. Garofalo, Plasma Phys. Controlled Fusion **43**, 1425 (2001).
[31]Y. Q. Liu, A. Bondeson, M. S. Chu, J.-Y. Favez, Y. Gribov, M. Gryaznevich, T. C. Hender, D. F. Howell, R. J. La Haye, and J. B. Lister, Nucl. Fusion **45**, 1131 (2005).
[32]Y. Q. Liu, A. Kirk, and E. Nardon, Phys. Plasmas **17**, 122502 (2010).
[33]N. N. Gorelenkov, H. L. Berk, and R. V. Budny, Nucl. Fusion **45**, 226 (2005).
[34]J. P. Graves, I. T. Chapman, S. Coda, L.-G. Eriksson, and T. Johnson, Phys. Rev. Lett. **102**, 065005 (2009).
[35]J. P. Graves, Plasma Phys. Controlled Fusion **55**, 074009 (2013).
[36]F. Porcelli, R. Stankiewicz, W. Kerner, and H. L. Berk, Phys. Plasmas **1**, 470 (1994).
[37]R. G. Littlejohn, J. Plasma Phys. **29**, 111 (1983).
[38]C. T. Hsu, Phys. Fluids B **2**, 280 (1990).
[39]G. Y. Fu, C. Z. Cheng, and K. L. Wong, Phys. Fluids B **5**, 4040 (1993).
[40]M. Rosenbluth and M. L. Sloan, Phys. Fluids **14**, 1725 (1971).
[41]Y. Liu, Nucl. Fusion **50**, 095008 (2010).
[42]T. Casper and A. Polevoi, ITER Documentation No. 2V3FDF, 2009.
[43]G. V. Pereverzev, Report No. IPP5/42, 1991.
[44]C. M. Fransson, B. Lennartson, C. Breitholtz, A. Bondeson, and Y. Q. Liu, Phys. Plasmas **7**, 4143 (2000).
[45]A. Bondeson, Y. Q. Liu, C. M. Fransson, B. Lennartson, C. Breitholtz, and T. S. Taylor, Nucl. Fusion **41**, 455 (2001).
[46]J. R. Drake, P. R. Brunsell, D. Yadikin, M. Cecconello, J.-A. Malmberg, D. Gregoratto, R. Paccagnella, T. Bolzonella, G. Manduchi, L. Marrelli, S. Ortolani, G. Spizzo, P. Zanca, A. Bondeson, and Y. Q. Liu, Nucl. Fusion **45**, 557 (2005).
[47]Y. Q. Liu, M. S. Chu, A. M. Garofalo, R. J. La Haye, Y. Gribov, M. Gryaznevich, T. C. Hender, D. F. Howell, P. De Vries, M. Okabayashi, S. D. Pinches, and H. Reimerdes, Phys. Plasmas **13**, 056120 (2006).
[48]J. P. Graves, O. Sauter, and N. N. Gorelenkov, Phys. Plasmas **10**, 1034 (2003).
[49]Y. Liu, M. S. Chu, W. F. Guo, F. Villone, R. Albanese, G. Ambrosino, M. Baruzzo, T. Bolzonella, I. T. Chapman, A. M. Garofalo, C. G. Gimblett, R. J. Hastie, T. C. Hender, G. L. Jackson, R. J. La Haye, M. J. Lanctot, Y. In, G. Marchiori, M. Okabayashi, R. Paccagnella, M. Furno Palumbo, A. Pironti, H. Reimerdes, G. Rubinacci, A. Soppelsa, E. J. Strait, S. Ventre, and D. Yadykin, Plasma Phys. Controlled Fusion **52**, 104002 (2010).